Narrowband Radar System for Indoor Doorway Detection

YUNXIANG LIU

School of Electrical and Electronic Engineering

Jan 2015

Acknowledgments

There are many people who helped me, encouraged me, cheered me up during my MEng program. I would like to thank them one by one here.

First, I would like to express my deepest gratitude to my supervisor Prof. Yong Liang GUAN for his unreserved support and patient guidance all the way through the course of this research. Learning from his solid research skills, open-mindedness and integrity in research has led me more mature in research. More importantly, learning from the way he treats others makes me become a more mature person, who should have a kind heart and be considerate for others.

Second, I am extremely thankful for my co-supervisor Prof. Dmitriy Garmatyuk, a visiting professor at NTU, from Miami University. This research would not reach its current level without his guidance, valuable suggestions and encouragement.

Third, I would like to express my gratitude to my former supervisor, Prof. Gang WU at National Key Laboratory of Science and Technology on Communications in University of Electronic Science and Technology of China (UESTC), what I have to mention is that it was him who offered me the opportunity of coming to NTU.

A big "thank you" also goes to Dr. Francois Quitin, who is a Research Fellow in INFINITUS lab. After my Qualifying Examination (QE), he gave me a lot of valuable suggestions and discussions.

Now it is the turn to say "thank you" to all the friends I have made over the years in Singapore, who have given me their help and support whenever I need, brought me a lot laugh and made my life more enjoyable and colorful.

At the end of this acknowledgement, I need to thank the most important persons in my life, who have given me all they have. They are my grandparents, parents and my fiancee (Pang Dudu). What I have owed to them is beyond what is possibly to be described by using any human language. I just wanna say "I love all of you so much" to them.

Contents

Abstract

Radar is an object-detection system that uses radio waves to determine the range and direction of objects. It could be employed on an Unmanned Ground Vehicle (UGV) for autonomous navigation. Although the UGV could sense the surrounding environment by using optical sensors such as camera or infrared sensors, these sensors may not work well in some environments, such as an environment with low visibility or an environment with obstacles made of transparent or polished materials. In these cases, radar sensors could be employed along with these optical sensors to enhance the navigation capability of an UGV.

To investigate this, a low-cost narrowband radar system based on USRP (Universal Software Radio Peripheral) hardware and C++/MATLAB programming is implemented to enable UGV autonomous indoor navigation. The main purpose is to investigate open doorway detection in an indoor environment utilizing a narrowband radar, which could be used for the UGV to detect the open doorway and navigate itself autonomously through the doorway.

We first present the design and calibration of a power-based narrowband radar system. It was found that, when the radar faces the wall, the relation between the received power and the distance to the wall follows the free-space path loss equation, rather than the traditional radar equation. This is due to the fact that the wall is too large to be treated as a point scatterer, and is better approximated by an infinite reflecting surface. We also present the design and validation of

radar ranging. The radar ranging algorithm was verified in three conditions, 1) using cables (to avoid multipath and self-interference problems), 2) in an anechoic chamber (to avoid multipath) and 3) in a real indoor environment. The test results show that the ranging error is approximately 50cm and the maximum detection range is up to 6 meters.

To detect an open doorway with an UGV, a "2-step" doorway detection procedure is utilized in this thesis. In the first step ("Step 1"), the nearest wall is detected by using a detection method called Shortest Range Determination (SRD). Then, in the second step ("Step 2"), an open doorway is detected by using the radar and a power-based detection algorithm to scan the space parallel to the nearest wall detected in the first step. This detection algorithm is based on total variation de-noising. It detects an open doorway by detecting the cross-range of the positions of the leftmost and rightmost sides of the open doorway. The experimental results give a detection error of around 30cm. Furthermore, when the robot scans the wall in "Step 2" , the range between the wall and the radar can be measured by using radar ranging process. By averaging all the reliable ranging values, the range between the robot and the wall is estimated to provide extra information of the doorway position. The doorway position coordinate is then built up by combining these information including the cross-range and the range of the doorway positions. Our approach to radar-assisted indoor positioning of an UGV is thus validated. Future research on this topic may include exploration of more complex scenarios (e.g. detection of signs of life amid rubble for UGV-based search-and-rescue missions), as well as enhancing the capabilities of the USRP-based system by fusing sensing and communications.

The main contributions of this work are

- the implementation, calibration and verification of the USRP-based radar system,

- the collection of open doorway detection data in realistic indoor environment,
- the design of effective radar processing algorithms,
- the demonstration of open doorway detection of radar-guided UGV.

List of Abbreviations

ADC	Analog to Digital Conversion
API	Application Programming Interface
AWGN	Additive White Gaussian Noise
CP	Cyclic Prefix
DAC	Digital to Analog Conversion
FSPL	Free-Space Path Loss
IBI	Inter Block Interference
MEng	Master of Engineering
OFDM	Orthogonal Frequency-Division Multiplexing
RF	Radio Frequency
RMS	Root Mean Square
ROS	Robot Operating System
RX	Reception, Receiver
SNR	Signal-to-Noise Ratio
SRD	Shortest Range Determination
TOA	Time of Arrival
TX	Transmission, Transmitter
UGV	Unmanned Ground Vehicles
UHD	USRP Hardware Driver
USRP	Universal Software Radio Peripheral
UWB	Ultra-Wide Band

VNA Vector Network Analyzer

List of Tables

List of Figures

Chapter 1

Introduction

1.1 Literature Review

Autonomous Unmanned Ground Vehicles (UGVs) are mobile platforms that serve a wide range of specialized applications in urban, military, domestic, and industrial settings [1]. They are designed to utilize a variety of sensors to navigate themselves in an unknown environment. To achieve this, vision systems, for example cameras, are employed for obstacle detection and environment mapping [2, 3, 4] while infrared sensors are used for range detection [5, 6]. Meanwhile, radar is also a promising sensor for autonomous UGV navigation purpose. It can complement other sensors which may have limitations due to certain surrounding environment and extend the range of applications for these UGVs.

UWB (Ultra-Wide Band) software defined radar is one of the options for the onboard radar system. In [7], an approach to indoor navigation, detection and room structure mapping was proposed and the detection method was verified by using a software-defined UWB OFDM (Orthogonal Frequency-Division Multiplexing) platform [8]. It uses the UWB OFDM platform as a custom-made imaging radar sensor system and uses a corner reflector to help the system to identify the open doorway. In addition, the authors also used these preliminary results to test the efficiency of detecting the presence and positions of the open doorway in [9].

As an alternative to the UWB software defined radar, a popular low-cost and computer-hosted software radio, USRP (Universal Software Radio Peripheral) platform, is another choice for the onboard radar system. Many researchers have built communications testbeds on this platform [10, 11, 12, 13, 14]. Although USRPs are not suitable for high resolution radar systems due to its bandwidth (maximum bandwidth is only 40 MHz for USRP N210), it can still find its place in many other radar applications. Several USRP-based radar systems have been successfully implemented and tested as reported in [15, 16, 17]. Authors of [15] used USRP for the implementation of a multiband passive radar. In [16], the authors have implemented a USRP-based frequency-modulated continuous-wave radar for the ranging detection in the weather surveillance application and, in [17], a car to car measurement testbed which employs a USRP-based OFDM radar was presented. All the proposed radar systems above only utilize radar ranging to detect the target of interest and the information of returned signal power is discarded in these works. In our proposed indoor radar system, the returned signals power is also used for detecting the target of interest, i.e. the open doorway in our case.

1.2 Motivation

Nowadays, an UGV (Unmanned Ground Vehicles) is able to navigate, detect and operate automatically. To achieve this, optical sensors (camera or infrared) are normally employed to detect the surrounding environment. However, UGV with such optical sensors may fail to navigate in some environments. For example, normal camera sensors do not work well in an environment of low-visibility or dark place, and it will be quite difficult for an infrared sensor to detect a glass door. What is even worse is that ghost reflection may happen to present wrong ranging information if the surface is polished. In these cases, a radar sensor may be able to detect the surrounding environment and provide useful information for navigation. Therefore, UGVs with both optical and radar sensors will be much more versatile.

Ultra-wide band (UWB) radar system works pretty well for indoor open doorway detection [7, 8, 9]. The detection of a clear open doorway in an indoor environment was verified by using both simulations and experiments. Nonetheless, the hardware of the UWB radar system is very expensive. This makes a low-cost narrowband USRP-based radar system attractive for implementing an UGV navigation system.

In this Master of Engineering (MEng) project we have investigated and overcome challenges that arise from using a low-cost narrowband USRP-based radar system for indoor navigation by an UGV. In particular, we focused on the open doorway detection problem in this thesis.

1.3 Objectives

The aim of this MEng project is to design a USRP-based radar system for detecting an open doorway in an indoor environment. The objectives of this research study are listed as follows:

- to design a narrowband radar by using the USRP as the hardware platform, and MATLAB in conjunction with C++ as the programming language;
- to carry out field measurements and collect real radar signal data for detecting an open doorway in a realistic indoor environment;
- to develop an effective doorway detection algorithm to process the collected data and guide an UGV to find the doorway and move through it.

1.4 Contributions

The main contributions of this work are

- the implementation, calibration and verification of the USRP-based radar

system,

- the collection of open doorway detection data,
- the design of effective radar processing algorithms,
- the demonstration of the open doorway detection of radar-guided UGV.

We adopted the OFDM pilot symbol waveform of the 802.11p standard as the radar signature waveform and we developed a MATLAB program to detect its arrival time and returned signal power. In addition, we designed a USRP hardware radar transceiver using C++ programming. Then, power calibration and ranging verification were carefully performed for the radar system.

The collections of open doorway detection data were performed in the Research Techno Plaza, level 4. A total of 25 sets of doorway detection profiles along with other measurement results were collected.

A 2-step doorway detection procedure was proposed along with the power-based doorway position detection algorithm and radar ranging processing. All these detection information were combined to determine the doorway position coordinates.

Two conference papers, which are based on the work above, have been published/accepted. They are

- Y. Liu, Y. L. Guan, and D. Garmatyuk, J. Morton "*USRP based OFDM radar systems for doorway detection*," in *IEEE Radar Conference*, 2014.
- Y. Liu, Y. L. Guan, D. Garmatyuk, F. Quitin, " *Improved Exit Path Identification with Indoor USRP-based Radar System*," to appear in *ION Pacific PNT* 2015.

1.5 Organization of the Report

The organization of the thesis is as follows:

Chapter 2 introduces the radar basics, including range determination, range resolution, range accuracy, free-space path loss function and radar equation. The functions of USRP, the antennas and radar waveforms are also briefly introduced. Furthermore, a detailed literature review on the related UWB radar system based doorway detection is presented.

Chapter 3 discusses the implementation, calibration and verification of the proposed radar system. The transmission power and receiving power are calibrated by the oscilloscope and the signal generator respectively. In addition, radar ranging is verified:

- with cables (to avoid multipath and self-interference problems);
- in an anechoic chamber (to avoid multipath);
- in a real indoor environment.

Chapter 4 presents measurement results of the proposed USRP-based radar system for doorway detection. A "2-step" doorway detection procedure is utilized. Meanwhile, we discuss the power-based doorway position detection method and radar ranging method as well as their corresponding algorithms. Then the combination of these methods is developed and discussed.

Chapter 5 demonstrates a USRP-based radar-guided UGV. In collaboration with a FYP (Final Year Project) student, we demonstrate that the UGV equipped with radar sensors is able to autonomously detect an open doorway successfully.

Chapter 6 concludes this thesis and propose possible future works.

Chapter 2

Background

2.1 Introduction

In this chapter, some background information on several fundamental concepts related to the narrowband radar system under study is presented. This includes

- The basic radar principle is presented followed by detailed radar range determination along with the concepts of range resolution and range accuracy, which defines the radar ranging performance. OFDM waveforms are also introduced because they can be used in the waveform designs for radar and communication systems. In addition, the path loss function and radar equation are discussed, where the findings of the relationship between wall reflection power and these functions will be presented in Chapter 3.

- USRP hardware and the associated software, upon which the radar transceiver is built, are introduced. The horn antenna, which is used as the directional antenna for the proposed narrowband radar system, is also introduced for the completeness of this thesis.

- The Pioneer 3-AT robot along with its software Robot Operating System (ROS) are introduced. This platform is employed as an Unmanned Ground Vehicle (UGV) and mounted with the proposed narrowband radar system to perform indoor open doorway detection.

- Total variation de-noising is introduced. It is employed to remove the noise without losing the step-like information in the power-based doorway detection profile, which we will discuss in Chapter 4.

- We also give a detailed literature review for the related works on UWB (Ultra-Wide Band) radar system based open doorway detection. Please note that we investigate a narrowband radar-based indoor open doorway detection in this thesis, which is an alternative choice to these Ultra-Wide Band radar-based systems.

2.2 Radar Basics

RAdio Detection And Ranging (RADAR) is an object-detection system that utilizes radio waves to determine the range, altitude, direction, or speed of objects [18]. In this section, some fundamental principles of a radar system are introduced.

2.2.1 Range Determination

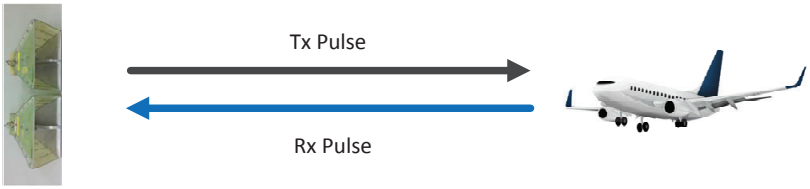

Figure 2.1: Radar Principle

A radar system uses electromagnetic waveforms (pulses) to detect objects. It transmits these radio-frequency (RF) waveforms into the detection space of interest, which are reflected by objects including the targets. Some of the reflected waveforms, which bounce off the target, travel back to the radar. These reflected waveforms are called an echo. A radar system is illustrated in Fig. 2.1, in which the target, an airplane, is detected by the radar using the returned signals. The time required for this signal to travel from the radar to the target and back again

is called the round trip delay time. It can be converted into the range (distance) between the radar and the target as follows:

$$R = \frac{c \cdot t}{2} \tag{2.1}$$

where c is the speed of light and t is the round trip time. Consequently, by applying this formula, we could determine the distance between the radar and the target once the round trip delay time is known. In the next section, the calculation of round trip delay time is described along with the range resolution and range accuracy.

2.2.2 Range Resolution and Range Accuracy

Range resolution is the ability of a radar system to distinguish between two or more targets on the same bearing but at different ranges [19]. The range resolution depends on the width of the transmitted pulse, the types and sizes of targets, and the efficiency of the receiver and indicator. Among all these factors, the width of the transmitted pulse is most crucial. A well-designed radar system, with all other factors at maximum efficiency, should be able to distinguish targets separated by one-half the pulse width time. Therefore, we could formulate the range resolution as:

$$Range_{res} \geq \frac{c \cdot \tau}{2} \tag{2.2}$$

where $Range_{res}$ denotes the range resolution, c is the speed of light and τ is the pulse width. Moreover, the pulse width of a baseband signal approximately equals to the reciprocal of its bandwidth, i.e. $\tau \approx B^{-1}$ [20]. Then the range resolution could also be formulated in frequency domain perspective as:

$$Range_{res} \geq \frac{c}{2 \cdot B} \tag{2.3}$$

where B is the bandwidth of the signal. The radar cannot distinguish any two objects, between which the distance is within the range resolution, which is discussed

in details next.

One commonly used pulse detection method is named as Matched Filtering, which is optimal for detecting the presence of reflected pulses in AWGN (Additive White Gaussian Noise). If the radar pulse signal is indicated as $p(t)$, the received signal is shown as

$$r(t) = \sum_{n=1}^{N} \sigma_n p(t - t_n) \tag{2.4}$$

Then matched filtering method is performed as

$$s_{mf} = p(t) * p^{\dagger}(-t) = \sum_{n=1}^{N} \sigma_n p(t - t_n) * p^{\dagger}(-t) \tag{2.5}$$

where we assume that there are N targets (objects) within the antenna radiation pattern, which have round trip delays $t_1, t_2, ..., t_N$ and reflected magnitudes $\sigma_1, \sigma_2, ..., \sigma_N$ respectively. The operator $*$ and superscript $\dagger$ denote convolution and complex conjugate respectively.

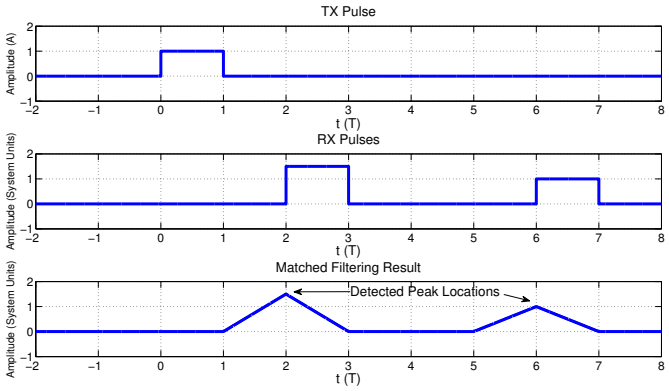

Figure 2.2: TX Pulse, RX Pulses and Matched Filtering Result

For the purpose of illustration, we assume that the transmitting pulse $p(t)$ is a rectangular pulse of amplitude A and duration T. Also, $p(t)$ starts at $t = 0$. An example is illustrated in Fig. 2.2, where there are two noise-free reflection pulses starting from $t = 2T$ and $t = 6T$. Matched filtering is performed for the received signals and the output results is shown in Fig. 2.2. It is shown that two distinguishable peaks are present in the matched filter output as the distance

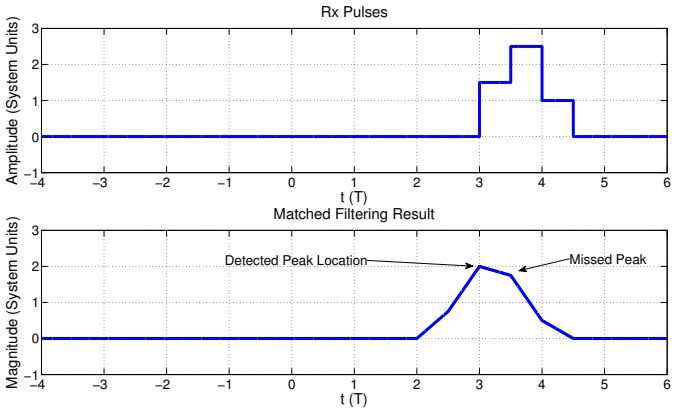

Figure 2.3: RX Pulses and Matched Filtering Result

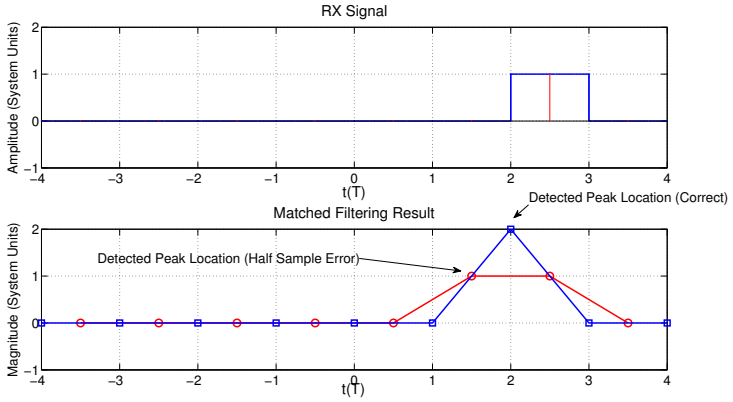

Figure 2.4: Range Accuracy Illustration

between two targets is greater than the range resolution. Then, the round trip delay is determined by reading off the time index of the corresponding peak point assuming that the time of transmission is at $t = 0$. However, in Fig. 2.3, two received pulses appear from $t = 3T$ and $t = 3.5T$ respectively. The distance between these two targets is smaller than the range resolution. As a result, the two peaks in the matched filter output overlap with each other as shown in Fig. 2.3. Then the matched filtering method can not produce two clear peaks for detection and the receiver can not distinguish them.

Range accuracy, which indicates the accuracy of range values, is another crucial parameter associated with range determination. For a finite bandwidth radar waveform, the detection of its received signals is performed by using a matched

filter, and the round trip delay time is determined by searching for the peak value of the matched filter output. Since all the signal processing is done digitally, we need to sample the analog received waveforms. The interval between radar samples in the receiver affects the range accuracy and is mainly determined by the sampling rate employed by the receiver. The CRLB (Cramer-Rao Lower Bound) [21, 22, 23, 24], which is a lower bound of any unbiased estimator, is present as the lower bound of range accuracy [21], followed by the introduction of the upper bound of range accuracy.

Suppose that a signal pulse $p(t)$ is transmitted. The round trip delay τ_0 from the transmitter to the target and back is related to the range R as $\tau_0 = 2R/c$, where c is the speed of light. Estimation of range is therefore equivalent to estimation of the time delay, assuming that c is known. Hence a model under AWGN channel is considered and the received continuous waveform $r(t)$ is

$$r(t) = p(t - \tau_0) + w(t) \qquad 0 \leq t \leq T. \tag{2.6}$$

where the transmitted signal pulse $p(t)$ is assumed to be nonzero over the interval $[0, T_i]$. Moreover, the signal bandwidth is assumed to be B Hz. $w(t)$ is bandlimited AWGN, which results from filtering the continuous waveform to the signal bandwidth of B Hz. The continuous received waveform is sampled at $S \cdot B$ Hz (S is the oversampling factor) so samples are taken every $T_s = 1/(S \cdot B)$ seconds to form the observed data

$$r(nT_s) = p(nT_s - \tau_0) + w(nT_s) \qquad n = 0, 1, ..., N - 1. \tag{2.7}$$

Letting $r[n]$ and $w[n]$ be the sampled sequences, we have our discrete data model

$$r[n] = p(nT_s - \tau_0) + w[n] \tag{2.8}$$

Note that $w[n]$ is WGN and the variance of $w[n]$ is $\sigma^2 = N_0 B$.

It should be noted that the form of general CRLB for signals in white Gaussian

noise [21] is formulated as

$$var(\hat{\theta}) \geq \frac{\sigma^2}{\sum_{n=0}^{N-1}\left(\frac{\partial p[n;\theta]}{\partial \theta}\right)^2} \tag{2.9}$$

Then we can apply (2.9) in evaluating the CRLB:

$$var(\hat{\tau_0}) \geq \frac{\sigma^2}{\sum_{n=0}^{N-1}\left(\frac{\partial p[n;\tau_0]}{\partial \tau_0}\right)^2} \tag{2.10}$$

$$= \frac{\sigma^2}{\sum_{n=n_0}^{n_0+M-1}\left(\frac{\partial p(nT_s-\tau_0)}{\partial \tau_0}\right)^2} \tag{2.11}$$

$$= \frac{\sigma^2}{\sum_{n=n_0}^{n_0+M-1}\left(\frac{dp(t)}{dt}\Big|_{t=nT_s-\tau_0}\right)^2} \tag{2.12}$$

$$= \frac{\sigma^2}{\sum_{n=0}^{M-1}\left(\frac{dp(t)}{dt}\Big|_{t=nT_s}\right)^2} \tag{2.13}$$

where $n_0 = \tau_0/T_s$ is the delay in samples and M is the length of the sampled signal. If we assume that T_s is small enough to approximate the sum by an integral, we have

$$var(\hat{\tau_0}) \geq \frac{\sigma^2}{\frac{1}{T_s}\int_0^{T_i}\left(\frac{dp(t)}{dt}\right)^2 dt} \tag{2.14}$$

Noting that $\sigma^2 = N_0 B$, we have

$$var(\hat{\tau_0}) \geq \frac{T_s N_0 B}{\int_0^{T_i}\left(\frac{dp(t)}{dt}\right)^2 dt} \tag{2.15}$$

As we know that the energy ξ is

$$\xi = \int_0^{T_i} p^2(t)dt \tag{2.16}$$

which results in

$$var(\hat{\tau}_0) \geq \frac{BT_s}{\frac{\xi}{N_0}\overline{F^2}} \tag{2.17}$$

$$= \frac{2BT_s}{\frac{\xi}{N_0/2}\overline{F^2}} \tag{2.18}$$

where

$$\overline{F^2} = \frac{\int_0^{T_i}\left(\frac{dp(t)}{dt}\right)^2 dt}{\int_0^{T_i} p^2(t)dt} \tag{2.19}$$

$$= \frac{\int_{-\infty}^{\infty}(2\pi F)^2|P(F)|^2 dF}{\int_{-\infty}^{\infty}|P(F)|^2 dF} \tag{2.20}$$

where F denotes continuous-time frequency, and $P(F)$ is the Fourier Transform of $p(t)$.

The term $\frac{\xi}{N_0/2}$ indicates a SNR. Moreover, $\overline{F^2}$ is a measure of the bandwidth of the signal, i.e. mean square bandwidth of the signal.

Finally, by noting that $R = c\tau_0/2$, the CRLB for range is

$$var(\hat{R}) \geq \frac{c^2 BT_s/2}{\frac{\xi}{N_0/2}\overline{F^2}} \tag{2.21}$$

The lower bound of range accuracy, i.e. range estimation error, is given by the standard deviation of CRLB as follows:

$$\delta_{Accu} \geq \frac{c\sqrt{BT_s/2}}{\sqrt{\frac{\xi}{N_0/2}}\overline{F}} \tag{2.22}$$

From (2.22), the larger the mean square bandwidth or the smaller the sample duration is, the smaller the lower bound of range accuracy will be. Furthermore, the larger the SNR is, the smaller the lower bound of range accuracy will be. As a result, we can decrease the lower bound of range accuracy by either increasing the transmitted signal bandwidth or shortening the sample duration, i.e. increasing the sampling rate in the RX.

Moreover, the range accuracy is upper bounded by the sampling rate employed by the receiver if it is a noiseless channel, since the ranging information is determined by searching for the peak points and calculating the round trip time of these echos as explained above. This is given by

$$Range_{UpAcc} = \frac{c}{2 \cdot R_s} = \frac{c \cdot t_s}{2} \tag{2.23}$$

where R_s denotes sampling rate and t_s denotes sampling duration. $Range_{UpAcc}$ denotes the upper bound of range accuracy.

Furthermore, the relationship between the sampling rate in the receiver and the bandwidth of the signal could be formulated as:

$$R_s = S \cdot B \tag{2.24}$$

where S denotes the oversampling factor.

Then we could formulate the upper bound of range accuracy in frequency domain perspective as:

$$Range_{UpAcc} = \frac{c}{2 \cdot S \cdot B} \tag{2.25}$$

Fig. 2.4 shows a case that the sampling rate used by the receiver is same as the bandwidth of the transmitted waveform. The blue circles are obtained when we happen to sample at the start point of the pulse, which is the perfect case, while the red circles are obtained when the detected peak position has an error of half sample duration because the peak point is shifted one half sample duration due to finite sampling rate and inaccurate sampling instants. It is clear that we may have a maximum error of one sampling interval and the corresponding range error is calculated by (2.23). Therefore, in order to improve the range accuracy, we need to increase the sampling rate used by the receiver to obtain a more accurate starting point detection. For example, assuming that the bandwidth of transmitted pulse is 10 MHz, the upper bound of radar range accuracy, i.e. the maximum ranging error,

is 15 meters if we sample the received radar waveform with the same sampling rate of 10 MHz. However, if we oversample the received waveform at 100 MHz, then the upper bound of range accuracy is improved to 1.5 meters. It should be note that the upper bound of range accuracy gives the maximum ranging error if direct matched filtering in a noiseless channel is performed without any interpolation.

2.2.3 Radar Waveform

In this project, an OFDM waveform is used as the radar signature waveform. One example of an OFDM radar waveform is illustrated in Fig. 2.5. Based on (2.5) ,the results of matched filtering of this waveform is presented in Fig. 2.6, in which the peak point represents the starting time of the pulse. Then the τ parameter in range resolution is illustrated in the "Zoom In" sub-plot of Fig. 2.6.

In our implementation, the bandwidth of the OFDM radar waveform is 10 MHz. According to (2.3), the range resolution is 15 m. Besides, the range resolution could also be determined by the sample duration 10^{-6} s based on (2.2), which also gives the same result of 15 m.

On the other hand, range accuracy is highly related to the signal bandwidth and sampling rate used by the receiver. The signal bandwidth B is 10 MHz and the root mean square bandwidth of the signal $\overline{F}$ is calculated to be 15×10^6 rad/s based on (2.19). In order to improve our range accuracy, we increase the sampling rate $1/T_s$ to 25 MHz ($S \cdot B = 2.5 \cdot 10$ MHz) in the receiver. Moreover, the SNR in the indoor detection environment ranges from 26 dB to 40 dB according to the experiment result. Hence, from (2.22) , the lower bound of range accuracy ranges from 45 cm to 9 cm. Moreover, the sampling rate in the receiver also gives a range accuracy upper bound of 6 m based on (2.23) or (2.25). However, the range accuracy of 6 m (if direct matched filtering is performed without any interpolation) is not accurate enough for the task of indoor doorway detection. Meanwhile, we do not aim to increase the range accuracy by increasing sampling rate due to the

hardware limitation and the purpose of investigating narrowband radar. Therefore, a quadratic interpolation-based estimation algorithm [25] will be utilized to further improve the ranging performance, i.e. approach the lower bound of range accuracy. More details can be found in Section 3.5.

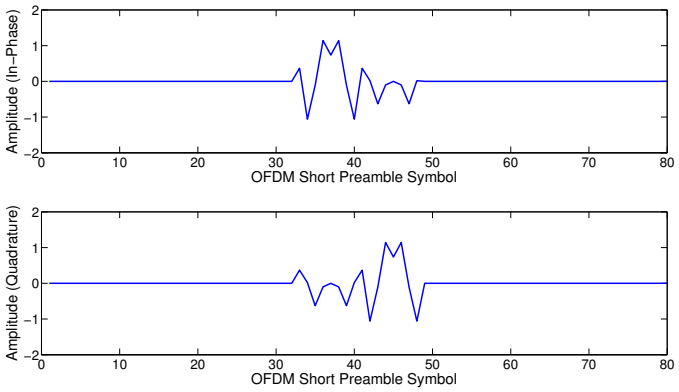

Figure 2.5: OFDM Radar Waveform (I and Q)

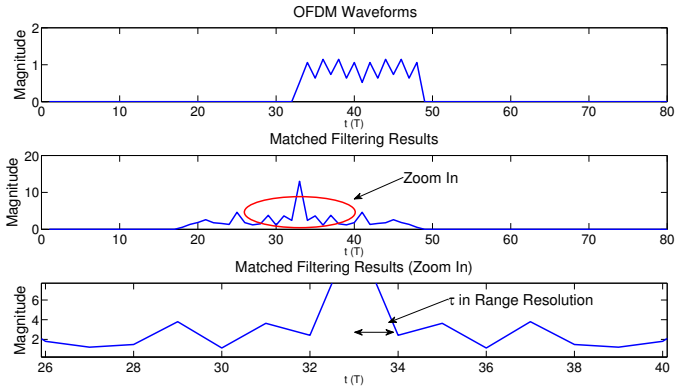

Figure 2.6: Matched Filtering of OFDM Radar Waveform

2.2.4 Path Loss Function and Radar Equations

Path Loss Function

Free-Space Path Loss (FSPL) is the loss in signal strength of an electromagnetic wave that would result from a line-of-sight path through free space, with no obstacles nearby to cause reflection or diffraction [26, 27]. Vacuum has the ideal conditions for measuring FSPL.

To begin with, we assume that the microwave signal energy is emitted by an isotropic radiator, which means that the energy propagates uniformly in all directions [27]. Areas with the same power density therefore form spheres around the radiator. The same amount of energy spreads out on an incremented spherical surface at an incremented spherical radius, hence the power density on the surface of the sphere is inversely proportional to the surface area A (or the square of the radius R) of the sphere. The detailed derivation of free space path loss function is presented as follows:

First, the spreading out of electromagnetic energy in free space is determined by the inverse square law, i.e

$$S = \frac{P_t}{4 \cdot \pi \cdot R^2} \tag{2.26}$$

where P_t is the transmitted power. The power per unit area at distance R is denoted as S, while R indicates the distance between transmitter and receiver.

Once the electromagnetic signal reaches the received antenna, the received power is also determined by the receiving antenna's aperture, which describes how well an antenna can pick up power from an incoming electromagnetic wave. As we assume that the antenna is isotropic, the received power is given by

$$P_r = \frac{S \cdot \lambda^2}{4 \cdot \pi} \tag{2.27}$$

where the received power is denoted as P_r and λ is the transmitted wave length.

In conclusion, the received power is given by:

$$P_r = \frac{P_t \cdot \lambda^2}{(4 \cdot \pi \cdot R)^2} = \frac{P_t \cdot c^2}{(4 \cdot \pi \cdot R \cdot f)^2} \tag{2.28}$$

By following the derivation above, it can be found that the expression for free space loss function actually encapsulates two effects. The first one is that the received power is inversely proportional to the square of the distance between the transmitter and receiver and the second one is that it is also proportional to the

square of the transmitted wave length, i.e. inversely proportional to the square of the frequency of the radio signal.

If directional antennas with antenna gain G_t and G_r for TX and RX antenna respectively are considered, then the modified free space loss function is given by:

$$P_r = \frac{P_t \cdot G_t \cdot G_r \cdot \lambda^2}{(4 \cdot \pi \cdot R)^2} = \frac{P_t \cdot G_t \cdot G_r \cdot c^2}{(4 \cdot \pi \cdot R \cdot f)^2} \tag{2.29}$$

Radar Equation

The radar equation describes the relation between the transmitted power and received power under certain propagation environment for a radar system. Radar sends out the electromagnetic waves, which are reflected if they meet an electrically leading surface [27]. Once the reflected electromagnetic waves are received again by the radar system, then a target is detected to be present in the transmitting direction. The reflected power is determined by radar equation [18]

$$P_r = \frac{P_t \cdot G_t \cdot G_r \cdot \lambda^2 \cdot \sigma}{(4\pi)^3 \cdot R^4} \tag{2.30}$$

where σ is the radar cross section, or scattering coefficient, of the target.

We can see that the received power is proportional to R^4 in (2.30) instead of R^2 as shown in (2.27). We will come back to this topic when we discuss the maximum radar sensing range in Chapter 3.

2.3 Radar Hardware and Software

We choose the Universal Software Radio Peripheral (USRP) Network series, i.e. N210 shown in Fig. 2.8, as the platform for the transceiver implementation. It is connected to a host computer, which is employed for signal processing, through a Gigabit Ethernet link. In TX, the generation of radar signals is done in laptop and the signals are sent to USRP via Ethernet cable. Then the signals in USRP are

modulated using a suitable carrier frequency after the Digital to Analog Conversion (DAC) and low pass filtering. The received signals are down-converted to baseband first in RX, followed by low pass filtering and Analog to Digital Conversion (ADC). After that, the signals are sent to the laptop via Ethernet cable and all the radar signal processing works are done in the laptop. A block diagram is shown in Fig. 2.7 [28, 29].

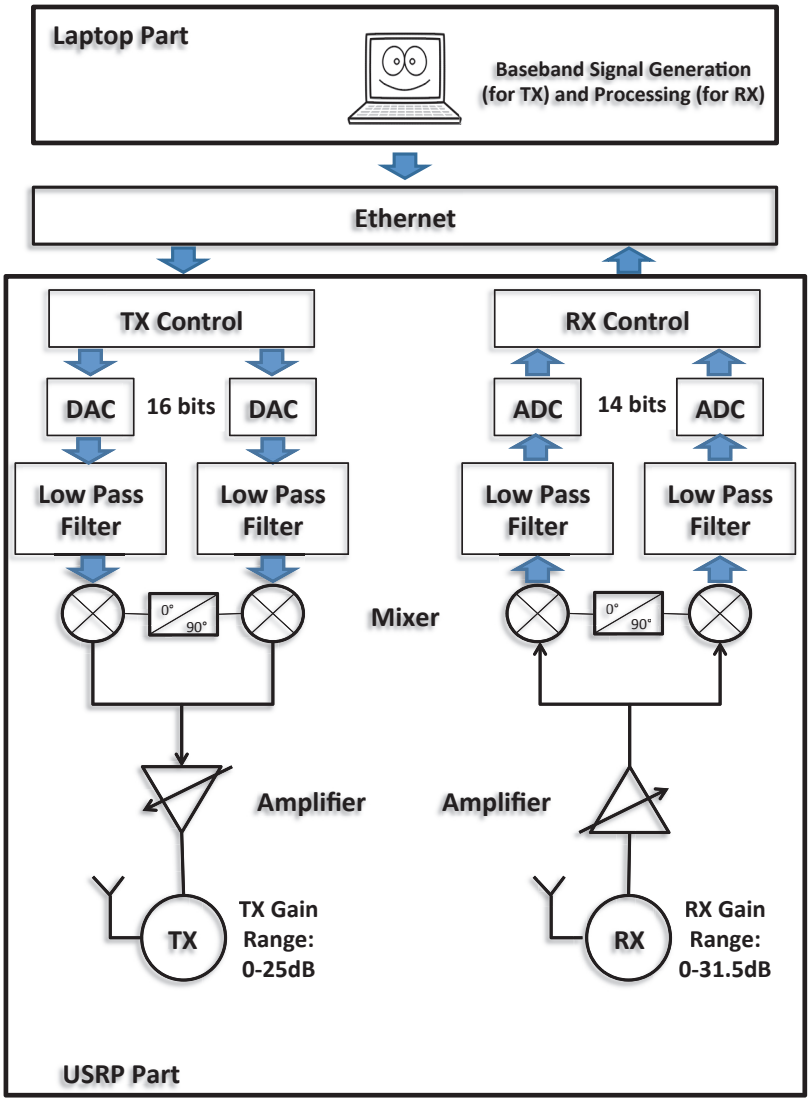

Figure 2.7: Block Diagram of Radar Hardware

The USRP products are computer-hosted software radios, which are inexpensive hardware platforms for software radio [30]. The Network Series, on which our radar system are built up, are the USRP board families having high-bandwidth,

high-dynamic range processing capability. They are suitable for applications requiring high RF streaming. Network series come with high resolution ADC and DAC for demanding applications. They also have higher bandwidth and dynamic range capability [31, 28]. As a result, it is suitable for narrow-band radar system [1]. USRP N210 along with the WBX daughterboard is utilized in our proposed radar system, whose hardware details are shown in Fig. 2.7. The center frequency ranges from 50 MHz to 2200 MHz and the bandwidth capability is up to 40 MHz. Moreover, the WBX daughterboards support full duplex operation.

Figure 2.8: USRP N210

Horn antennas[2] are employed as directional antennas for the proposed USRP-based radar system. To be specific, the JXTXLB series broadband waveguide horn antennas are used. The JXTXLB series broadband waveguide horn antennas are linearly polarized and can provide an efficient low cost means of making broadband measurements [32]. The frequency range that horn antenna can cover

[1]Although our radar is narrow band, it always holds true that the higher the bandwidth the better range resolution and range accuracy. Thus we have chosen Network Series as the USRP platform because it has the highest bandwidth

[2]Horn antennas, instead of printed circuit antennas, are employed in the proposed radar system to suppress the fading effect and direct coupling effect. More details can be found in Appendix A. We suggest that the reader first gets a clear view of the proposed open doorway detection by going through Chapter 3 and Chapter 4 before reading the Appendix.

is from 200 MHz to 40 GHz. These horns are ideally suited for EMI testing, direction finding, surveillance, antenna gain and pattern measurements and other applications. The JXTXLB series horn antennas can offer high gains, over octave bandwidths, low VSWR and advantages of having small sizes and light weight [32]. Fig. 2.9 shows the horn antenna (Model number: JXTXLB-10180) that we used for the doorway detection experiment. The antenna gain at 2 GHz carrier frequency of this horn antenna is 10.25 dBi. Moreover, the radiation pattern of this horn antenna at 2 GHz carrier frequency is shown in Fig 2.10 [32].

MATLAB and C++ are the programming language used to control the USRP hardware as well as process the baseband signal. USRP Hardware Driver (UHD) provides an application programming interface (API), which provides access to various functions of the USRP including synchronization, sample streaming and configuration [33]. Lots of code examples written by C++ are provided with the UHD that allows basic functional testing of USRP devices. In our implementation, a C++ code example named "txrx_loopback_file" is employed and modified to make the USRP device working as a radar transceiver. Moreover, MATLAB programming is employed to process the baseband signals. Besides, a binary file is used in between the MATLAB and C++ programming as the interface. In short, C++ programming is utilized for RF-end control while MATLAB programming is utilized for baseband signal processing in the laptop.

2.4 Unmanned Ground Vehicle

In this section, we will introduce the UGV used for the prototyping of radar-guided UGV. The UGV we employ is the Pioneer 3-AT [34], which is shown in Fig. 2.11. It is a four wheel drive robotic platform, software-compatible with all MobileRobots robots [34]. It is capable of carrying a payload of up to 12 kg, which is very crucial because the horn antennas in our proposed radar system are relatively heavy.

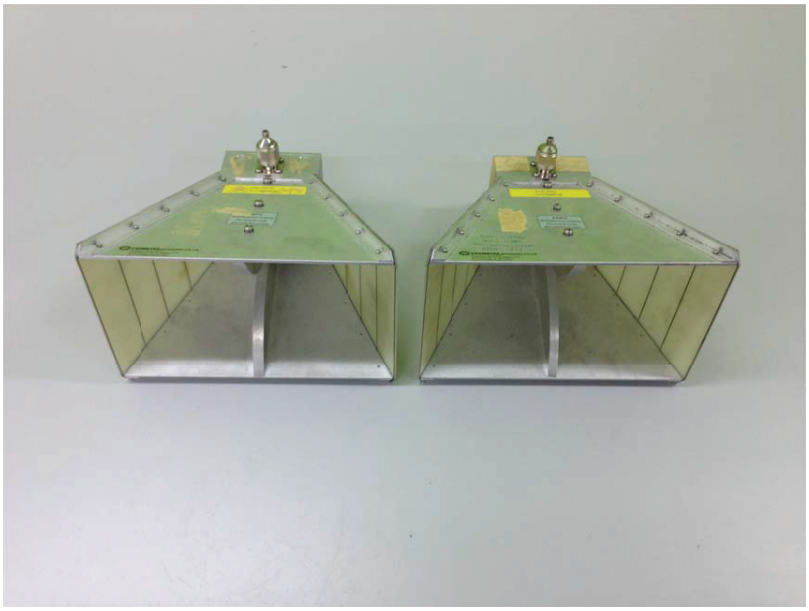

Figure 2.9: Horn Antenna

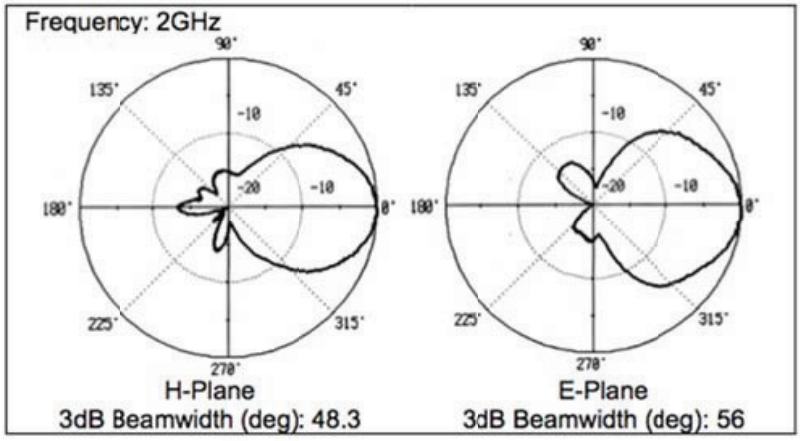

Figure 2.10: Radiation Pattern of Horn Antenna

Besides, the Robot Operating System (ROS) is the associated software used to control the Pioneer 3-AT. This system is a flexible framework for writing robot software [35]. It is a collection of tools, libraries, and conventions that aim to simplify the task of creating complex and robust robot behavior across a wide variety of robotic platforms. Furthermore, ROS support from MATLAB is used to control the Pioneer 3-AT [36]. By doing so, the Pioneer 3-AT could be controlled via m-file programming in MATLAB. The velocity, the angular velocity and the time could be specified. Besides, MATLAB is employed as the interface between

Figure 2.11: Pioneer 3-AT

the Pioneer 3-AT and the radar system, which will be discussed in Section 5.2.

2.5 Total Variation De-noising

Total variation de-noising [37] is a process that could remove the noise in step-like signals without losing the step-like information. We will exploit this method to remove the noise contained in the power-based doorway detection profile in Chapter 4. The basic principle of this process is that signals with excessive and possibly spurious details have high total variation, so the integral of the absolute gradient of the signal is high. In [38], it was shown that total variation de-noising could remove the noise from step-like signals which are highly discontinuous, even at low Signal-to-Noise Ratio (SNR). The basic mathematical description is given as follows:

For a digital signal y_n, the total variation is defined as:

$$V(y) = \sum_n |y_{n+1} - y_n| \tag{2.31}$$

Given an input signal x_n, the goal of total variation de-noising is to find an approximation that has smaller total variation than x_n but is "close" to x_n. This approximation is denoted as y_n. One measure of closeness is the sum of square errors:

$$E(x, y) = \frac{1}{2}\sum_n (x_n - y_n)^2 \tag{2.32}$$

So the purpose of total variation de-noising problem is to minimize the following discrete functional over the signal y_n:

$$E(x, y) + \lambda \cdot V(y) \tag{2.33}$$

where the parameter λ governs the relative importance of the total variation term compared with the sum-of-squares error term, which needs to be tuned empirically.

Once the parameter λ is fixed, by minimizing this convex function, an optimal solution y_{opt} could be found. For example, an illustration of step-like function is shown in Fig. 2.12(a), in which the red line and the blue line denote noiseless and noised step-like signal respectively. Then the total variation de-noising process is applied to remove the noise of the blue line without losing the step-like information, in which the parameter λ is manually set to be 100 for illustration purpose. For our practical application, the optimal λ is found by minimizing the RMS error of all the collected doorway detection experiment results. The de-noised profile is presented in Fig. 2.12(b), which results in a similar structure of the step-like function shown as red line in Fig. 2.12(a). It clearly shows that the noise is removed without losing the step-like information.

2.6 Related Work: Doorway Detection based on UWB Radar System

In [7], one of the early studies which addressed the open doorway detection problem by using a radar sensor was presented. A radar platform is placed in an empty

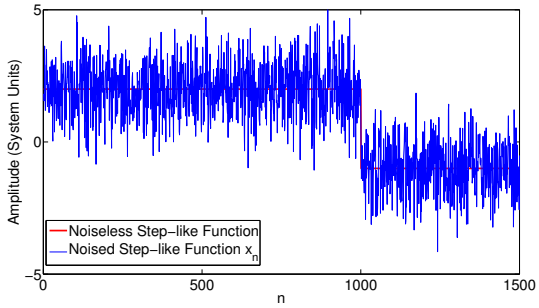

(a) Noiseless and Noised Step-like Functions

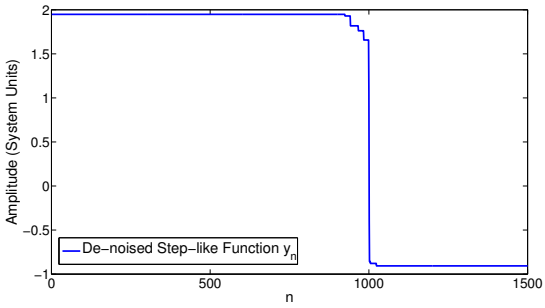

(b) Total Variation De-noised Step-like Function ($\lambda = 100$)

Figure 2.12: Illustration of Step-like Function

room (only wall, no obstacles) with an open doorway and the goal was to locate the doorway position. A simple initialization period is adopted, during which the radar spins while transmitting. During each single turn, a simple ranging algorithm is performed to determine the direction that gives the shortest detected range. This is treated as the nearest wall. Then the system orients the radar so that it can transmit the signal perpendicular to the closest wall. This enables the radar to move parallel to the wall. Then the return power from the radar-illuminated area, which is used for doorway detection, is estimated by calculating the moments of the received signals based on known models of the environment's components. According to the authors' simulation results, the open doorway is successfully located with good accuracy if the SNR level is equal or above 0 dB. Furthermore, this result was verified in [8]. A software-defined UWB OFDM radar system is utilized to detect the location and dimensions of doorways using the generalized likelihood ratio test. The authors in [9] extended these preliminary results further to test the efficiency of detecting the presence and positions of the open doorway. It was shown that the position of the width of the doorway was accurately estimated in a typical indoor environment with measurement step sizes of 15 in or less.

Chapter 3

Calibration and Verification of Narrowband Radar System

3.1 Introduction

The main focus of this chapter is the calibration and verification of the proposed narrowband radar system. As shown in Fig. 3.1, the proposed radar system consists

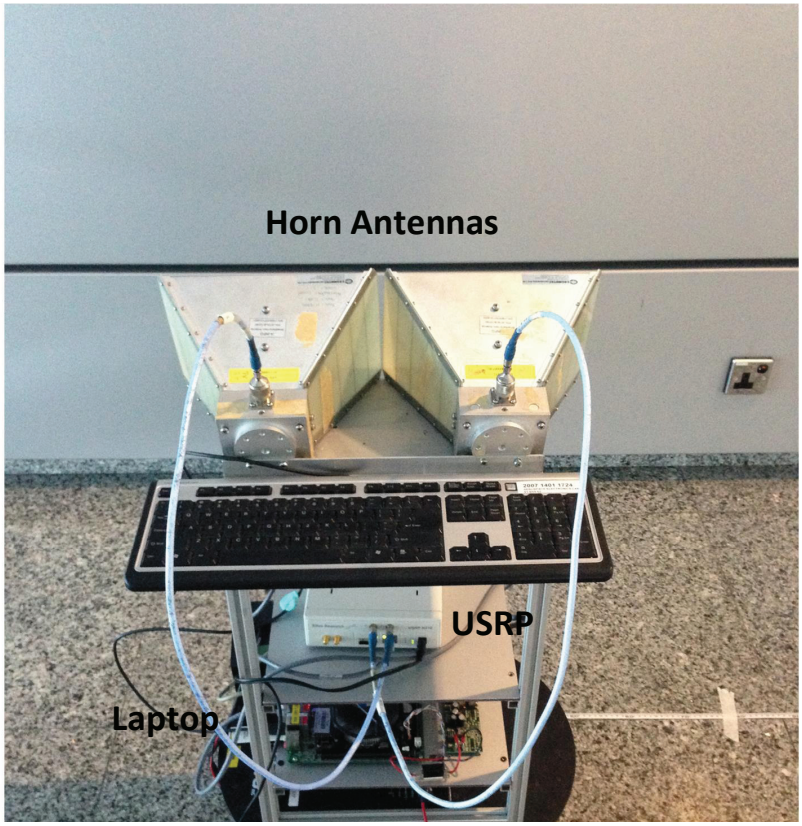

Figure 3.1: Illustration of Radar System

of a USRP N210, which is equipped with a WBX daughterboard allowing the signal transmission and reception at a frequency of 2 GHz. A laptop is used to process the baseband signals and control USRP N210 via a Ethernet connection. Two horn antennas (introduced in Section 2.3) are attached to the USRP as TX and RX antennas.

We first introduce the calibration for a power-based radar system. The TX and RX power are calibrated by using an oscilloscope and a signal generator, respectively. Then, calibration of the direct coupling effect is performed in an anechoic chamber. The relationship between free-space path loss function and traditional radar equation is also discussed. Furthermore, the validation for radar ranging is presented. It is verified under three different settings, namely

- using cables (no multipath and self-interference),
- in an anechoic chamber (no multi-path),
- in a real indoor environment.

3.2 Power Calibration

In this section, we show how to calibrate the power of the proposed USRP-based radar system. The actual TX power varies between different USRP WBX daughterboards [39] and only the gain of TX (maximum gain is 25 dB) can be specified. Also, at the receiver side, USRP is not capable of measuring the received power level directly. Therefore, it is necessary to perform calibration for both TX power and RX power.

3.2.1 TX Power Calibration

In order to calibrate the TX power of the proposed radar system, the radar TX port is first connected to an oscilloscope via a low loss cable as shown in Fig. 3.2.

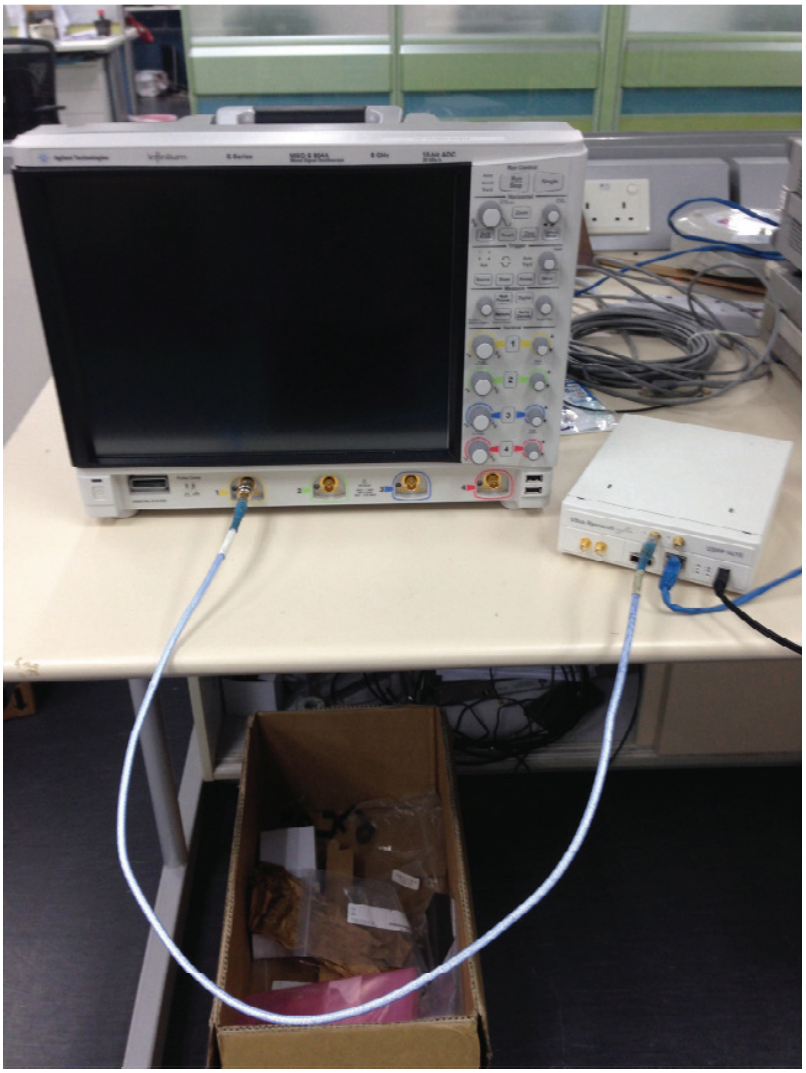

Figure 3.2: Illustration of TX Power Calibration

Then OFDM radar waveforms are transmitted with 25 dB TX gain and the Root Mean Square (RMS) voltage is measured by using the oscilloscope. So the TX power can be determined by the equation given by:

$$P = \frac{V_{rms}^2}{R_{Ohm}} \tag{3.1}$$

where the V_{rms} is defined as the RMS of the voltage, P denotes the average power and R_{Ohm} denotes the input resistance, which is 50 Ω for the oscilloscope used.

By doing so, we can determine the TX power, once the RMS voltage is measured by oscilloscope. In our experiments, the TX power of the proposed radar

system is 1.4 dBm. It will be used for the calibration of direct coupling effect later in Section 3.3.

3.2.2 Rx Power Calibration

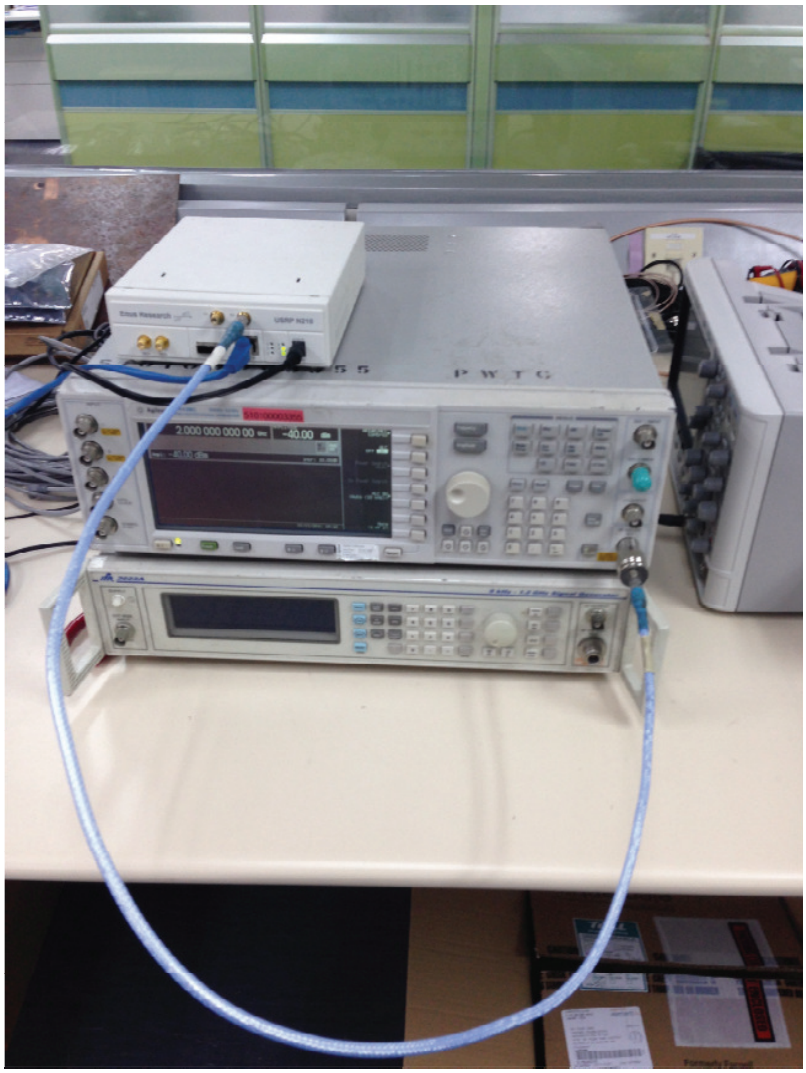

Figure 3.3: Illustration of RX Power Calibration

Since the USRP can not measure the received power directly, the amplitudes of the received signals do not have any physical meaning. In order to calibrate it, a signal generator is utilized to align the amplitude of received signals against the true power. The set up for RX power calibration is illustrated in Fig. 3.3. Signal generator transmits the pilot tone with different power levels, e.g. 0 dBm, -10 dBm, etc. The proposed radar system (RX Gain is set to 0 dB) receives the

Table 3.1: RX Power Calibration Results (RX Gain: 0 dB)

Signal Generator (True Power, dBm)		-60	-50	-40	-30	-20	-10	0
RX Signal Relative Power in dB	Trial 1	-51.3	-41.7	-31.8	-21.9	-11.9	-1.9	8.1
	Trial 2	-51.2	-41.8	-31.8	-21.8	-11.8	-1.9	8.1

pilot tone signals via the low loss cable and down converts the signal to baseband. The relative power of the sampled received signals is calculated by the following equation:

$$\hat{P} = \frac{1}{N}\sum_{n=1}^{N}|x_n|^2 \tag{3.2}$$

where $\hat{P}$ is defined as the relative power calculated in MATLAB, N denotes the length of the discrete signal and x_n is the amplitude of received signal sample. The relative power in dB is computed by using

$$\hat{P}_{dB} = 10 \cdot log_{10}(\hat{P}) \tag{3.3}$$

As the TX power is specified by signal generator, the calculated relative power of the received signal could be aligned against the true power. In Table 3.1, the first row represents the true power specified by signal generator while the bottom two rows denote two trials of measured $\hat{P}_{dB}$ calculated according to (3.2) and (3.3). The relationship is found out by subtracting the true power from the calculated relative power, for each trial and each power level. Then the mean value of the subtraction results of all the trials and power levels is computed, which is 8.24 dB according to the Table 3.1. Then the relationship between the true power and the calculated baseband signal relative power in dB is

$$P_{true} = \hat{P_{dB}} - 8.24 \tag{3.4}$$

where P_{true} denotes the true power in dBm.

Consequently, the power for any received signals of our proposed radar system could be computed according to (3.4). This will be used for the calibration of direct coupling effect in Section 3.3. It will also be employed for the RX power

measurement, which is used for power-based doorway detection in Section 4.3.

3.3 Direct Coupling Effect

Figure 3.4: Calibration of Direct Coupling Effect

As shown in Section 2.2.3, OFDM waveforms, rather than a short pulse, are utilized as the radar waveforms for the proposed radar system and two horn antennas are mounted side by side as TX and RX antennas. It should be noted that, since the TX antenna and RX antenna are working simultaneously at the same frequency and since the reflector (wall) is very close to the radar, the RX antenna will receive both the TX signals directly from the TX antenna (unwanted direct coupling signal) and the echos (desired radar signals). This phenomenon is called direct coupling. In this section, the direct coupling effect is carefully calibrated in an anechoic chamber to validate the feasibility of our radar system. Two calibration methods, using USRP and using VNA (Vector Network Analyzer), are proposed. Results obtained from using both methods are close to each other, which also validates the correctness of the power calibration process. The details of both calibration methods are given below

- **Calibrated with USRP:** In Section 3.2.2, the power of received signal is calibrated and can be calculated based on (3.4). It could be used to measure

the direct coupling. In order to keep the results uncluttered, the direct coupling effect is calibrated in the anechoic chamber as shown in Fig. 3.4. According to the measurement results, the RX power is -55 dBm while the TX power is 1.4 dBm. Therefore, the power difference between the RX and TX paths of our USRP radar is around -56.4 dB.

- **Calibrated with VNA:** In order to eliminate the effect of cable loss, the VNA is utilized to measure the S_{21} factor, which denotes the power difference between the RX and TX signals. As shown in Fig. 3.5, the S_{21} is around -58 dB. It is clear that this result is close to the one measured by using USRP, which implicitly validate the correctness of the power calibration. The cable loss is -56.4 - (-58) = 1.6 dB, which is reasonable.

In the proposed USRP-based radar system, the TX power is set to 1.4 dBm, so the direct coupling power is around -55 dBm [1], which includes cable loss. A 10 dB margin is set to prevent the received signal from being dominated by the direct coupling effect. So if the received power is lower than -45 dBm, we consider the received signal will be unreliable and the ranging information (discussed in Section 4.4) will be discarded. The influence of direct coupling on the maximum radar sensing range will be discussed in Section 3.4.

3.4 Free-Space Path Loss Function Vs Radar Equation

Normally, the relationship between TX power and RX power for a radar system is described by radar equation shown in (2.30). It is valid only when the target

[1]The direct coupling power of the proposed radar system mainly comes from two parts, i.e. the power leakage from TX to RX through horn antennas and the power leakage from TX to RX inside the USRP. In the case of attaching horn antennas, the power leakage inside the USRP dominates the direct coupling effect, while the power leakage from horn antennas is negligible. As a result, placing a metallic shield or an RF absorber cannot help reduce the direct coupling effect.

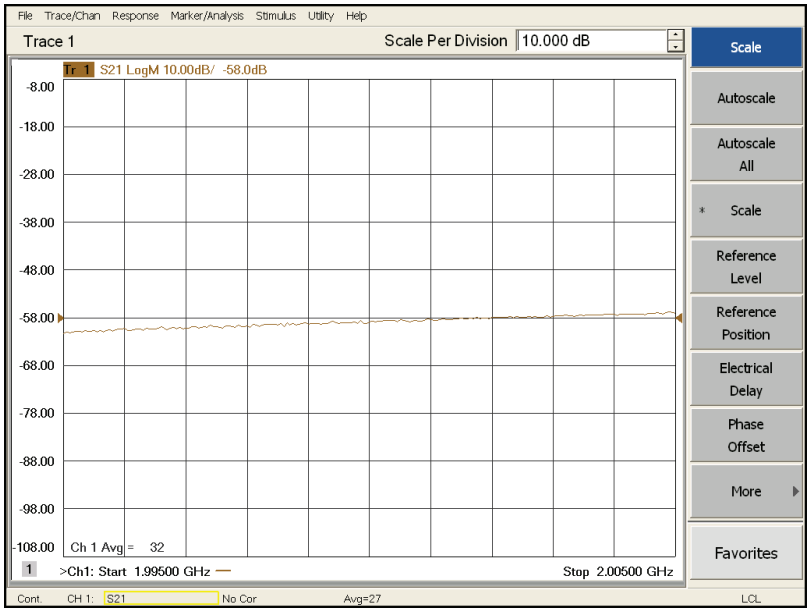

Figure 3.5: S_{21} Coefficients

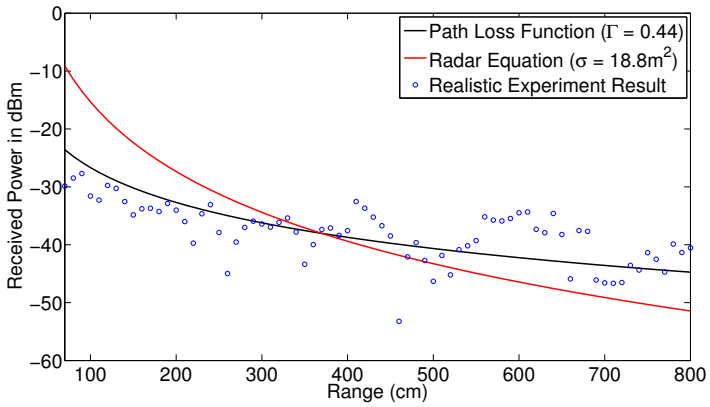

Figure 3.6: Path Loss Function Vs Radar Equation

is far from the radar, which means that the target reflects the TX signals like a point scatterer. However, our proposed radar system is used for short distance indoor navigation, where the target is a wall in front. Therefore the wall is better approximated by an infinite reflecting surface rather than a point scatterer and the free space path loss function [2] with a reflection factor Γ may fit this case well,

[2]In this section, we aim at showing that radar equation model is not suitable for indoor doorway detection scenario. Instead, free space path loss model gives a good approximation result. The reason that free space path loss model, rather than two-ray ground reflection model, is used to compare to the radar equation model is because free space path loss model gives better approximation in a short distance scenario compared with two-ray ground reflection model. More details can be found in Appendix B

Figure 3.7: Set up of the Power Measurement in a Realistic Environment

which is shown as:

$$P_r = \frac{P_t \cdot G_t \cdot G_r \cdot \lambda^2}{(4 \cdot \pi \cdot D)^2} \cdot \Gamma = \frac{P_t \cdot G_t \cdot G_r \cdot c^2}{(4 \cdot \pi \cdot D \cdot f)^2} \cdot \Gamma \tag{3.5}$$

where Γ is the reflection factor, $0 \leq \Gamma \leq 1$. It should be noted that $D = 2 \cdot R$, where R denotes the distance between the target and the radar.

This conjecture is verified by the realistic experiment results. To begin with, the proposed radar system faces the wall perpendicularly as shown in Fig. 3.7 and calculates the reflected signal power every 10cm apart. Then the collected signal powers from different distance to the wall are shown as blue circle in Fig. 3.6. By

minimizing the root mean square error of the path loss function model and radar equation model based on the realistic experiment results, the reflection factor for path loss function is found to be approximately 0.44 (black curve in Fig. 3.6)and the radar cross section is found to be 18.8 m^2 (red curve in Fig. 3.6). Intuitively, we can tell from Fig. 3.6 that the wall reflection model is better approximated by path loss function. Furthermore, the root mean square errors of path loss function model and radar equation model based on realistic experiment results are found to be 4.2 dB and 8.4 dB respectively, where the former is lower. As a consequence, the measurement results are better approximated by the free-space path loss function rather than the radar equation.

In addition, by using the free space path loss function with a reflection factor, the maximum radar sensing range could be determined. The reflection factor is set to 0.44 and the power threshold is set to -45 dBm (discussed in Section 3.3). According to (3.5), the maximum radar sensing range is 7.1 m. This result is verified in Fig. 3.6, which shows that the detection power is around -45 dBm when the detection range increases to 7.1 m.

3.5 Ranging Verification

The proposed radar system is expected to detect the distance between the wall and the radar to offer ranging information for open doorway detection task. It is implemented as follows: Frames of OFDM symbols with 10 MHz bandwidth using the carrier frequency of 2 GHz are transmitted. The received signals are oversampled at a symbol rate of 25 MHz. Matched filtering is then used to obtain the cross-correlation. According to (2.23) and 25 MHz bandwidth, the range accuracy is 6 meters, which is not accurate enough for indoor navigation. So a quadratic interpolation-based estimation algorithm [25] is utilized. It is well known that the auto-correlation of a band limited signal is symmetric around zero and the cross-

correlation in our case can be expressed in terms of the auto-correlation of the TX signals, which leads to the symmetric properties around the peak point. Then the cross-correlation function around the peak can be approximated by a parabola of the following form:

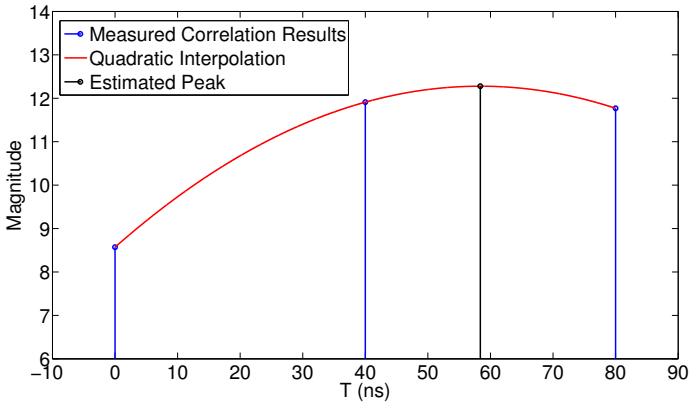

Figure 3.8: An Example of Quadratic Interpolation

$$C_D(\tau) = a\tau^2 + b\tau + c \tag{3.6}$$

Therefore, the Time of Arrival (TOA) lies in the apex of the parabola:

$$\tau = -\frac{b}{2a} \tag{3.7}$$

As a result, the peak point of the discrete cross-correlation samples and its two neighboring samples are inserted in (3.6). Then (3.7) is solved to yield the approximated peak of the cross-correlation, which is the estimation result. The round trip delay equals to the difference between the TX time and the location of estimated peak point. Consequently, estimated distance between the wall and the radar is computed based on (2.1). An interpolation example is shown in Fig. 3.8. The discrete correlation results around the peak point are shown as blue circle. The parabola approximation is shown in red line and the estimated peak point is shown as dark circle. Eventually this radar ranging method is verified in three setting, namely 1) using cables (to avoid multipath and self-interference problems), 2) in an anechoic chamber (to avoid multipath) and 3) in a real indoor environment.

The details of these verification procedures are shown in the following.

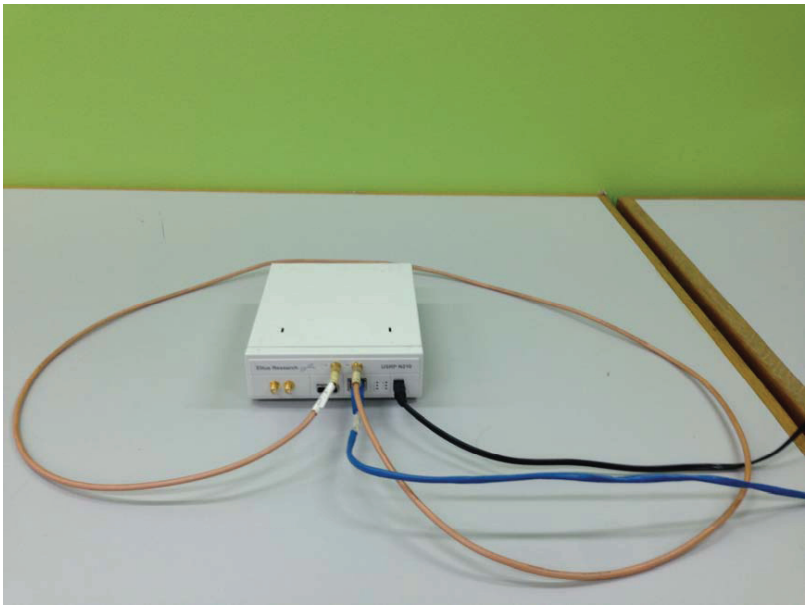

Figure 3.9: Set up of Ranging Verification with Cables

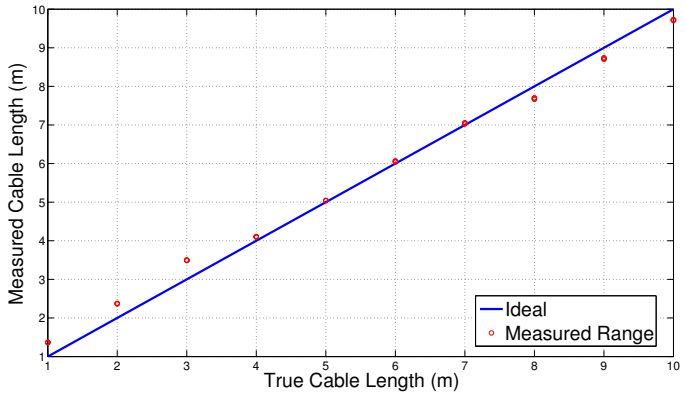

Figure 3.10: Results of Ranging Verification with Cables

- **Verified with Cables:** The radar ranging algorithm is first verified with cables as shown in Fig. 3.9. Multipath and self-interference (direct coupling) do not exist in this case because TX and RX ports are connected directly by using a cable, whose length is chosen from {1 m, 2 m, ..., 10 m}. The sampling rate in the RX is 25 MHz. Each length has totally 5 trials of experiment results, which are shown in Fig. 3.10. The experiment results for each length shown in Fig. 3.10 are obtained from total 5 trials. From these

measurements, the maximum estimation error is around 50 cm and the RMS error is 28.09 cm.

- **Verified in the Anechoic Chamber:** In the second setting, the radar ranging algorithm is verified in the anechoic chamber illustrated in Fig. 3.11. In this setting, multipath does not exist but self-interference, namely direct coupling effect, is present. Two horn antennas are attached to the USRP transceiver while a metal reflector is placed right in front of the radar. Then the measured range is verified at different distance shown in Fig. 3.12. By utilizing a sampling frequency of 25 MHz, the maximum estimation error is still around 50 cm. The RMS error is 35.08 cm because the fluctuation is more severe than the one with cables due to some direct coupling effect.

- **Verified in the Realistic Indoor Environment:** In the third setting, the ranging algorithm is tested in a realistic indoor environment as shown in Fig. 3.13. To begin with, the proposed radar system faces the wall perpendicularly. Then it moves further away from the wall perpendicularly and collects the reflected signals every 10 cm apart. Then the estimated distance to the wall is illustrated in Fig.3.14. The estimated ranging fluctuates a lot due to multi-path effect, which sometimes causes the received power to be lower than the -45 dBm threshold and hence discarded. The RMS error is 70.12 cm.

3.6 Concluding Remarks

In this chapter, the proposed radar system is carefully calibrated and verified. Our radar system is capable of computing the RX power and direct coupling effect, which determines the maximum radar sensing range. Furthermore, we found that the relationship between the RX power and the distance to the wall follows the free-space path loss function instead of the traditional radar equation because the

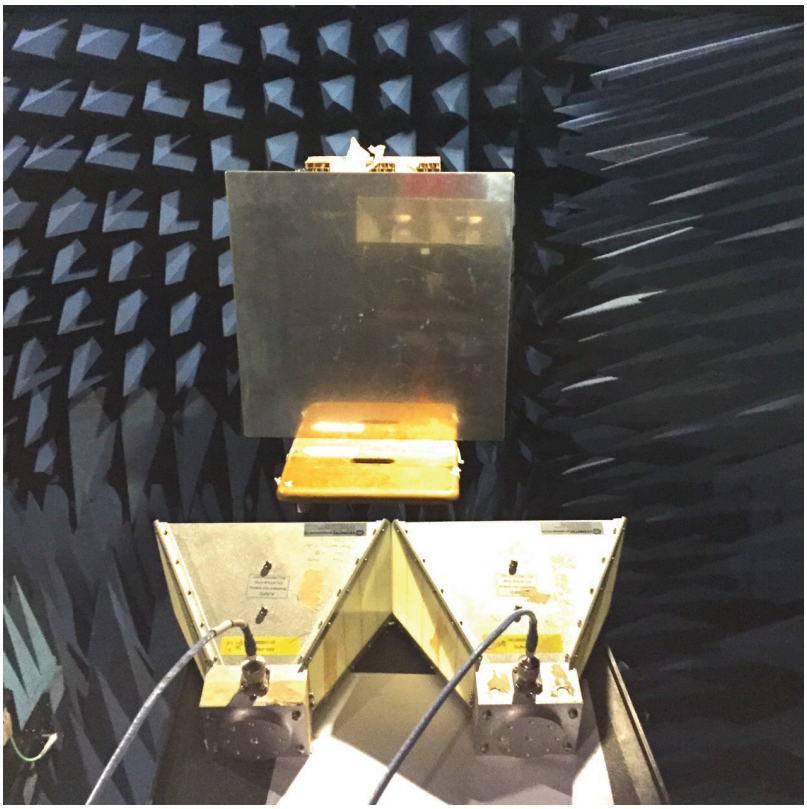

Figure 3.11: Set up of Ranging Verification in an Anechoic Chamber

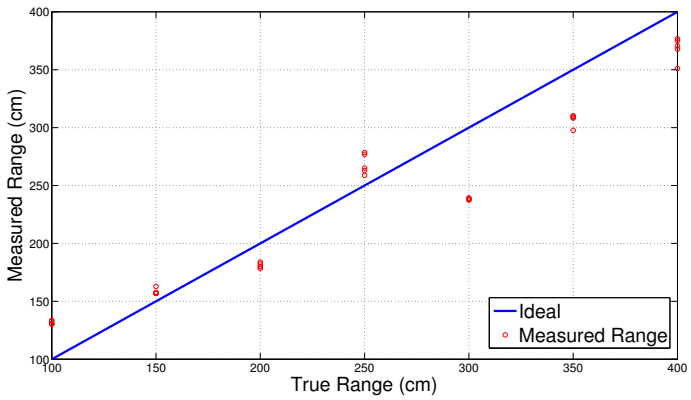

Figure 3.12: Results of Ranging Verification in an Anechoic Chamber

wall is better approximated by an infinite reflecting surface rather than a point scatterer. Finally, the radar ranging algorithm with quadratic interpolation is verified and the detection RMS errors are at most 70 cm.

Figure 3.13: Set up of Ranging Verification in a Realistic Indoor Environment

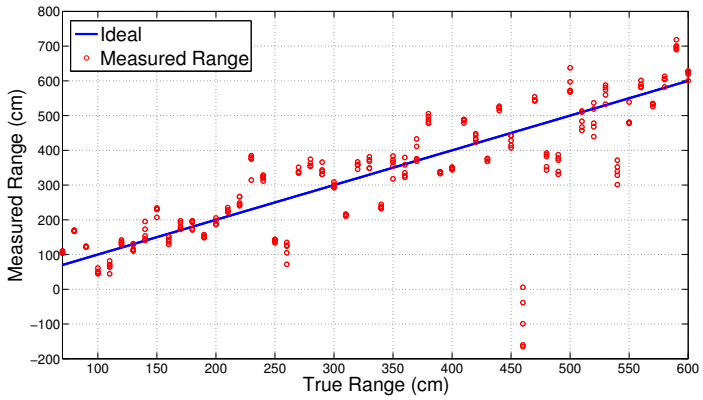

Figure 3.14: Results of Ranging Verification in a Realistic Indoor Environment

Chapter 4

Open Doorway Detection based on Narrowband Radar

4.1 Introduction

In this chapter, we investigate the open doorway detection in an indoor environment by utilizing the radar system proposed in Chapter 3. A straightforward doorway detection procedure [8] is considered, which can be decomposed into two steps. In the first step ("Step 1"), the nearest wall is detected by using a proposed detection method called Shortest Range Determination (SRD). Then, in the second step ("Step 2"), an open doorway is detected by scanning the space parallel to the detected nearest wall using radar sensors. For the second step, a power-based doorway detection method is proposed and corresponding doorway position detection algorithm is developed to estimate the position of the edges of the open doorway. In addition, the distance between the wall and the radar, which is estimated by using radar ranging, serves as an extra information for determining the doorway position. Then the doorway position coordinates are built up by combining all these informations. Field-tested experiments are carrier out and results are presented. Eventually the proposed doorway detection procedure is verified in another experiment site.

4.2 Doorway Detection Procedure

In this section, the indoor field test environment and doorway detection procedure are introduced. The proposed USRP-based radar system is mounted on an UGV, e.g. Pioneer 3-AT [34], which is in turn navigated using this radar sensor. All of our experiment data are collected by using the USRP as the RF front-end while all the signal processing works are done by using Matlab/C++.

Figure 4.1: Doorway Detection Environment

Fig. 4.1 shows the place where most of experimental data used in this work are collected. There is a door going through the wall nearest to the platform and the whole indoor environment is relatively clutter-free (no obstacles and large objects are present in radar detection path so that multi-path reflection is mainly caused by ceiling ,floor and corner). The doorway detection procedure, which is summarized in Fig. 4.2, can be divided into two steps as follows:

STEP 1:

At the starting point, the SRD algorithm is applied to find the direction along

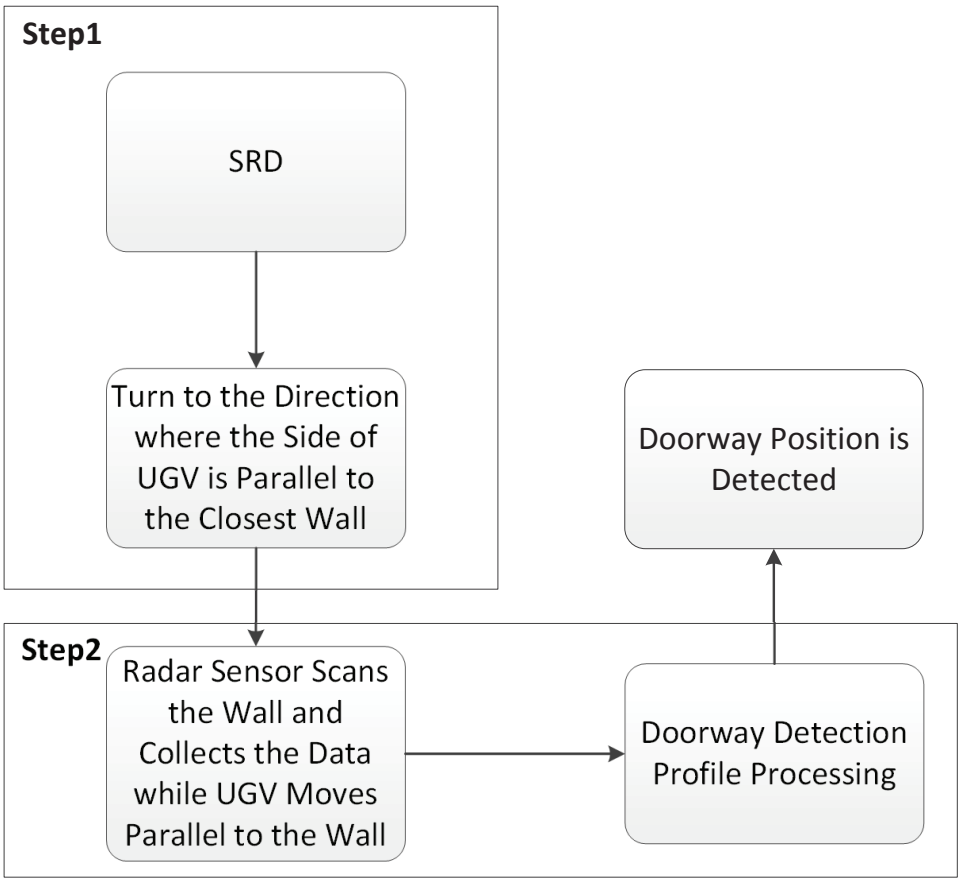

Figure 4.2: Doorway Detection Procedure

which the robot is perpendicular to the nearest wall. This is achieved by rotating the robot for one cycle 360° with a fixed step size (e.g. 5°) and the direction to the nearest wall is simply determined by the direction at which the returned signal power is the largest. Once this direction is determined, the robot will turn to the direction along which the side of robot is parallel to that wall.

STEP 2:

The robot then moves along that direction (parallel to the wall) while the radar sensor scans the wall until it reaches the end of this wall. The presence of an opening (doorway) is then detected. In this way, an open doorway can be detected by processing all these collected signals.

4.3 Power-based Doorway Detection

In power-based doorway detection, the radar system utilizes the returned signal power to find the nearest wall and the open doorway. This idea is based on the fact that the returned power is high when the radar faces a wall, and low when it faces an open doorway.

4.3.1 "Step 1" Measurements

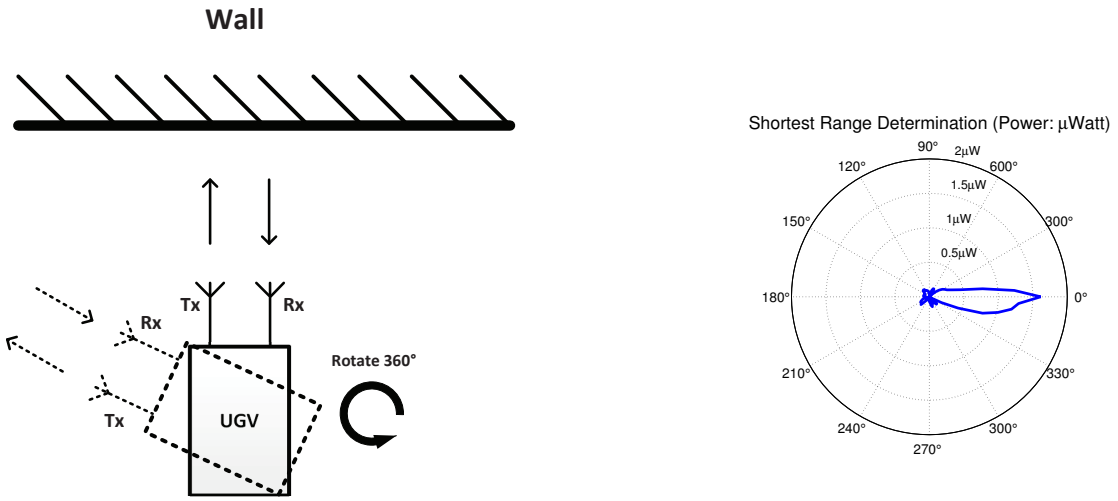

(a) Experimental Setup of SRD Measurement (b) Example of Results of SRD (Correct Nearest Wall Direction is at 0°)

Figure 4.3: Illustration of Shortest Range Determination (SRD)

In "Step 1", SRD is performed to find the direction perpendicular to the nearest wall. The USRP radar will be rotated for 360° and the returned signal power is measured as a function of the orientation angle of the radar as illustrated in Fig. 4.3(a). We determine the direction of shortest distance to the wall by finding the direction in which the largest returned signal power is received[1]. In the ideal scenario, if we assume that there is no noise presented and the radar beam width is extremely narrow, which looks like a laser, the returned signal power is expected to be highest when the radar is facing the wall perpendicularly. However, in a

[1]If the UGV is placed equidistant from two walls at right angles to each other, the proposed SRD will select the wall with higher returned signal power.

realistic indoor environment, due to multiple effects such as noise, finite antenna beamwidth, and fading, the SRD results may not be accurate. An example of SRD is illustrated in Fig. 4.3(b), where 0° is the correct wall direction. In this case, the nearest wall is quite distinguishable within acceptable detection error. Once the perpendicular direction facing the wall has been identified, the radar will be turned to a direction that is parallel to the wall before "Step 2" commences.

4.3.2 "Step 2" Measurements

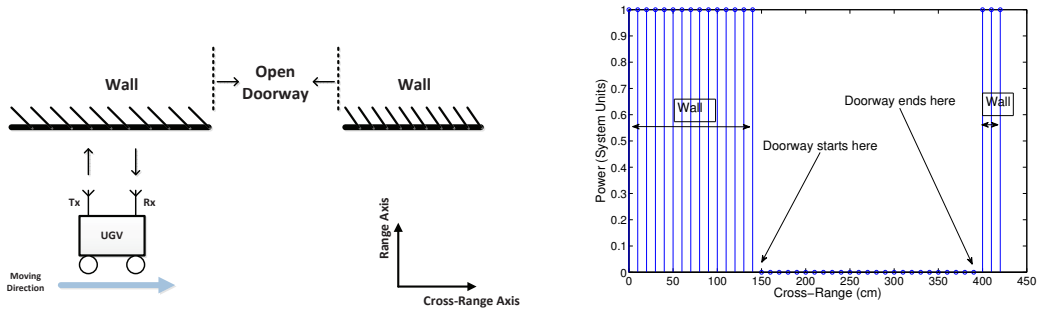

(a) Experimental Setup of Power-based Doorway Detection Measurement

(b) Ideal Power-based Doorway Detection Profile

Figure 4.4: Ideal Power-based Doorway Detection

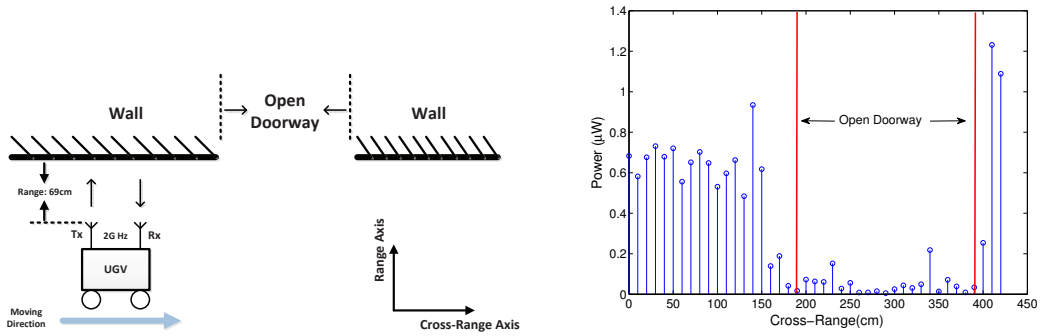

(a) Experimental Setup of Power-based Doorway Detection Measurement

(b) Example of Power-based Doorway Detection Profile

Figure 4.5: Power-based Doorway Detection at 69 cm with 2 GHz Carrier Frequency

In "Step 2", the radar will move in a direction that is parallel to the wall, which is shown in Fig.4.4(a). The returned signal power will be expected to remain roughly constant until the UGV is positioned in front of an open doorway.

At this position, the returned signal power will be expected to drop abruptly, e.g. Fig. 4.4(b). However, in practical measurements, the effects of multi-path fading and direct coupling are found to introduce random power fluctuations to the returned signal powers. The measurement results of one trial, which are collected by using 2 GHz carrier frequency, are shown in Fig. 4.5(b)[2] and the associated setup of this trial is shown in Fig. 4.5(a). As can be seen, the open doorway position is quite distinguishable despite the small power fluctuation due to many realistic factors including multi-path fading, direct coupling and noise.

In addition, the result obtained using SRD in "Step 1" may also contain errors due to the finite step size in angular rotation, e.g. the true nearest wall direction is 2 deg but the USRP starts at 0 deg and rotates at an interval of 5 deg. If this happens, the UGV will not move exactly parallel to the wall. As a result, the returned signal power may show some additional variations. To illustrate this, Fig.4.6(a) shows the movement of the UGV where a SRD error of 10° is presented and Fig. 4.6(b) shows the corresponding doorway detection profile at 2 GHz with a 10° SRD directional error, which causes the antenna to be moved away from the wall during scanning process. Due to the presence of SRD error, the distance between the radar and the wall varies while the radar scans the space parallel to the wall. As a result, the fading effect introduces more severe fluctuation.

4.3.3 Doorway Position Detection Algorithm

The basic idea for this algorithm is that because the returned power is high when the radar faces a wall and low when it faces an open doorway, an open doorway could be detected by finding the edges of the low power region in the power-based doorway detection profile. In this case, a Simple Doorway Detection Algorithm (SDDA) is proposed to determine the open doorway position by setting a threshold

[2]The "Cross-Range" axis in the power profile plots refers to the moving direction and the "Range" denotes the distance between the radar and the wall as shown in Fig.4.5(a)

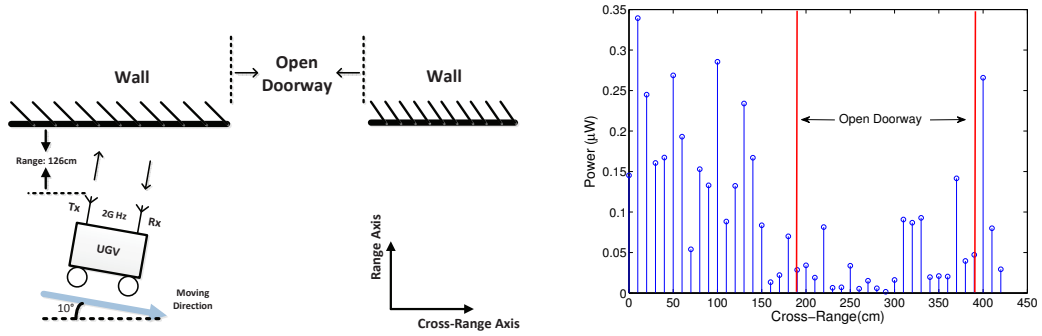

(a) Experimental Setup of Power-based Doorway Detection Measurement

(b) Example of Power-based Doorway Detection Profile

Figure 4.6: Power-based Doorway Detection Profile at 2 GHz with 10° SRD Error ("Range" Starts from 126 cm)

to classify whether the wall or an open doorway is faced by the radar.

Simple Doorway Detection Algorithm (SDDA)

The SDDA algorithm is developed based on simple threshold detection, which is described in details as follows:

A. Collect the power-based doorway detection profile via "Step 2";

B. Calculate the mean value of the detection profile P_{mean};

C. Fix the threshold scale parameter μ_{scale};

D. Calculate the threshold θ_{thre} as follows:

$$\theta_{thre} = \mu_{scale} \cdot P_{mean} \tag{4.1}$$

E. Set all the returned power that is smaller than θ_{thre} to be 0;

F. Consider each set of continuous "0" as a doorway position candidate set;

G. Choose the doorway position candidate set with largest number of elements as the doorway position set and treat the index of its first element and last

element as leftmost edge and rightmost edge for the open doorway respectively.

In the SDDA algorithm, it should be noted that the parameter μ_{scale} need to be carefully selected. In order to achieve the optimal performance, we focus on a metric of minimizing the mean square errors of detecting the doorway position based on all the experiment results. The error of doorway position detection is defined as follows:

$$Error = (S_{tr} - S_{de})^2 + (E_{tr} - E_{de})^2 \tag{4.2}$$

where S_{tr}, S_{de}, E_{tr} and E_{de} indicates the true doorway start point, the detected doorway start point, the true doorway end point and the detected doorway end point respectively.

By using all the experiment data collected to minimize this error function, the best μ_{scale} is found to be 1.732, and the mean square error equals to 16.25 cm.

Doorway Position Detection Results based on SDDA

Table 4.1: Doorway Position Detection obtained from Experiment Data - SDDA

Range to Wall	SRD Error	Measured Doorway Position (**True Position: 150cm-390cm**)				
		Trial1 (cm)	Trial2 (cm)	Trial3 (cm)	Trial4 (cm)	Trial5 (cm)
69cm	0°	160-400	150-390	150-390	150-390	150-390
126cm	0°	150-400	140-390	150-400	150-400	140-400
310cm	0°	120-380	140-400	120-380	140-410	140-390
Start from 69cm	5°	160-410	160-410	160-410	160-410	160-410
Start from 126cm	10°	140-390	140-390	140-390	140-390	140-390

The doorway position detection results based on SDDA are shown in Table. 4.1 and illustrated in Fig. 4.7. As can be seen, the detection results in short ranges to the wall are relatively better as SNR is higher. However, as the range to the wall increases, the detection results become worse because practical effects such as multi-path fading and direct coupling are not negligible anymore in low SNR region. Moreover, the error contributed by using SRD in "Step 1" may also intro-

duce high noise variance. For example, in Fig. 4.8(a), doorway detection profile at "Range" 310 cm is presented. There is an impulse noise at "Cross-Range" 340 cm. The SDDA algorithm may treat it as the rightmost edge, which causes large detection error. Consequently, a de-noising process is required to enhance the detection ability.

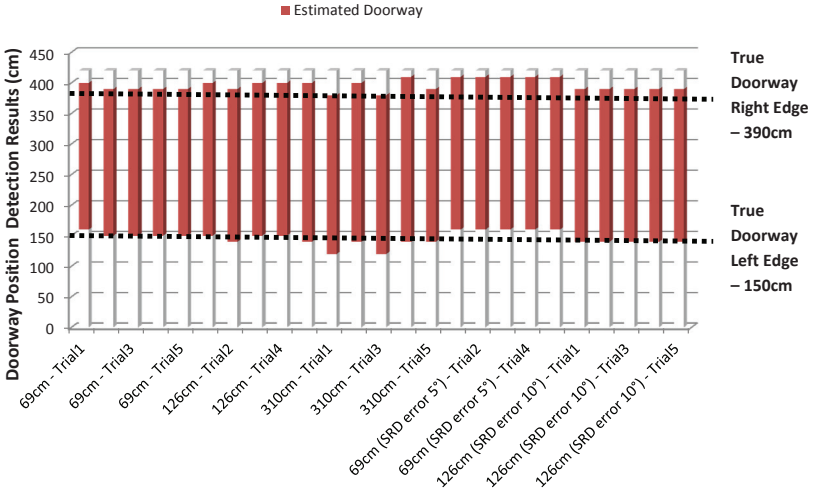

Figure 4.7: Illustration of Doorway Position Detection Results - SDDA

Total Variation De-nosing Algorithm (TVDA)

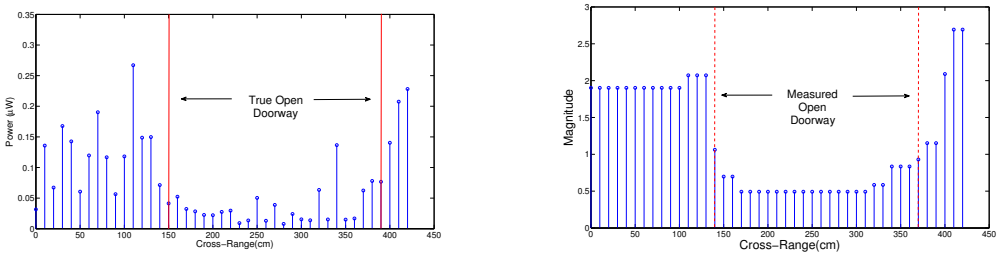

(a) Original Power-based Doorway Detection Profile - Range (Distance to the Wall): 310 cm

(b) De-noised Power-based Doorway Detection Profile ($\lambda = 2$ in (2.33))

Figure 4.8: Illustration of Total Variation De-noising

As discussed in previous section, high noise decreases the detection performance of the SDDA algorithm. In this section, a total variation de-noising process is developed to suppress the noise, especially impulse noise, but preserve the step-like information in the doorway detection profile. For instance, an example of

de-noised doorway detection profile is presented in Fig. 4.8(b). It shows clearly that the noise, especially the impulse noise shown at cross-range 340 cm, is removed by using the proposed total variation de-noising process. Therefore, by using the total variation de-noising process, we have improved the performance of the proposed doorway position detection algorithm. This de-noising process works as follows:

A. Collect the power-based doorway detection profile via "Step 2";

B. Fix the parameter λ and do the de-noising process by minimizing the cost function shown in (2.33);

C. Calculate the mean value of the de-noised detection profile P_{mean};

D. Fix the threshold scale parameter μ_{scale} and calculate the threshold as follows:

$$\theta_{thre} = \mu_{scale} \cdot P_{mean} \tag{4.3}$$

E. Set all values smaller than θ_{thre} to be 0;

F. Consider each continuous set of "0" as a doorway position candidate set;

G. Choose the doorway candidate set with largest number of elements as the doorway position set and treat the index of its first element and last element as leftmost edge and rightmost edge for the open doorway respectively.

Table 4.2: Doorway Position Detection obtained from Experiment Data - TVDA

Range	SRD Error	Measured Doorway Position (**True Position: 150cm-390cm)**				
		Trial1 (cm)	Trial2 (cm)	Trial3 (cm)	Trial4 (cm)	Trial5 (cm)
69cm	0°	160-400	150-390	160-390	160-390	150-390
126cm	0°	150-390	150-380	150-390	150-390	150-390
310cm	0°	120-380	140-390	140-370	150-410	140-370
Start from 69cm	5°	170-390	170-390	170-390	170-390	170-390
Start from 126cm	10°	150-390	150-390	150-390	150-390	160-390

For the TVDA algorithm described above, we adopt a metric of minimizing the mean square errors of detecting the doorway position based on all the experiment results in order to find the optimal parameters λ and μ_{scale}. The error function of doorway position detection defined here is the same as the one in Section 4.2. We iterate over different value of λ and μ_{scale} based on this error function. Then we choose the pair of λ and μ_{scale} which gives the best doorway position estimation. Processed with our power detection profiles, the best values of λ is 0.96-2.4, the best value of μ_{scale} is 0.88 and mean square error is 14.28 cm.

Doorway Position Detection Results based on TVDA

The doorway position detection results are shown in Table. 4.2 and illustrated in Fig. 4.9. It is better than the detection results of SDDA algorithm because the total variation de-noising process could remove the impulse noise in low SNR region. Furthermore, the main objective of open doorway detection is to ensure that the UGV goes through the door successfully. So we are more concerned with the doorway mid-point, whose results are shown in Table 4.3. In Fig. 4.10, the doorway mid-point detection error is also illustrated. As can be seen, the detection error is relatively small even if the range to the wall is large.

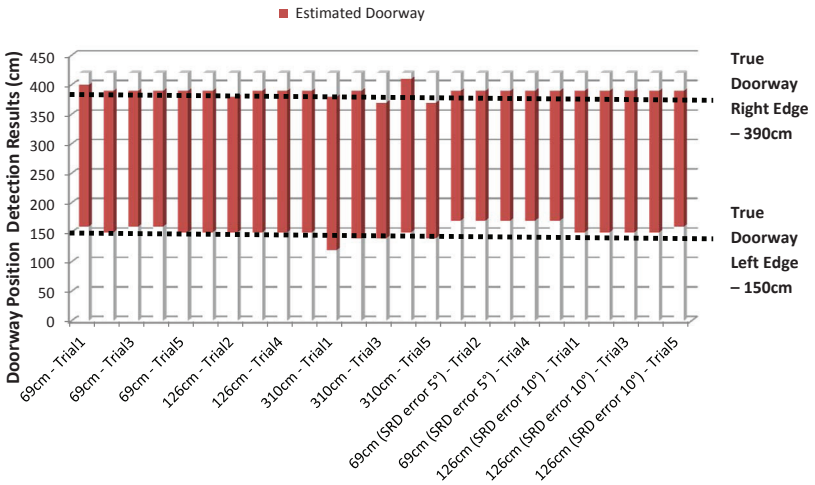

Figure 4.9: Illustration of Doorway Position Detection Results - TVDA

Table 4.3: Doorway Mid-point Measurement obtained from Experiment Data

Range	SRD Error	Measured Doorway Midpoint					
		Ideal	Trial1	Trial2	Trial3	Trial4	Trial5
69cm	0°	270cm	280cm	270cm	275cm	275cm	270cm
126cm	0°	270cm	270cm	265cm	270cm	270cm	270cm
310cm	0°	270cm	250cm	265cm	255cm	280cm	255cm
Start from 69cm	5°	270cm	280cm	280cm	280cm	280cm	280cm
Start from 126cm	10°	270cm	270cm	270cm	270cm	270cm	275cm

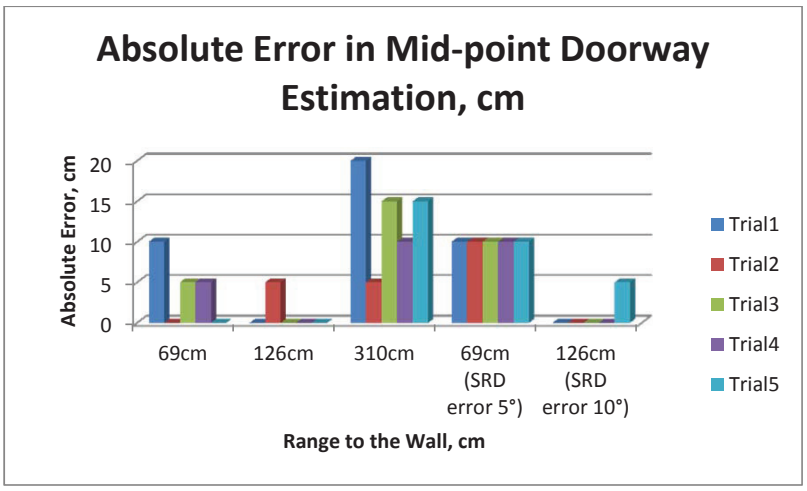

Figure 4.10: Illustration of Doorway Mid-point Detection Error

4.4 Radar Ranging for Doorway Detection

Recall that, in Section 4.3.3, the power-based doorway position detection is used for "Step 2" measurement, which provides the "Cross-Range" information of the doorway position. In this section, a radar ranging algorithm is developed to give "Range" information of doorway position, which is the distance between the wall and the radar. It should be noted that this ranging information is valid only when the radar is facing the wall and unreliable (hence invalid) when the radar faces an open doorway or when the received signal power drops below the threshold of -45 dBm at which the direct coupling effect is not negligible (discussed in Section 3.3). Consequently, the proposed algorithm is developed as follows:

A. Collect the power-based doorway detection profile via "Step 2";

B. All the detection points within the estimated doorway position are discarded;

C. All the detection points whose received power is less than -45 dBm are discarded;

D. Radar ranging are performed for the remaining detection points;

E. The final ranging information is acquired by taking the mean of all the ranging values left.

In this algorithm, the main purpose is to measure the distance between the wall and the radar. As can be seen, all the unreliable ranging information is discarded, including the detection points facing the doorway and the detection points whose received power is below the threshold of -45 dBm. The estimation results[3] are listed in Table. 4.4 and illustrated in Fig. 4.11. Besides, the results of radar ranging error are illustrated in Fig. 4.12. As can be seen, the detection error at 310 cm is larger compared with the results at 69 cm and at 126 cm because the SNR is lower and the multi-path fading effect is more severe in this case, which coincides with the lower bound of range estimation shown in (2.22) that higher SNR gives a lower estimation error. These range results also match our experience obtained from previous experiments in Section 3.5 that the radar ranging error of the distance to the wall is in sub-meters in realistic indoor environment[4].

[3]For the case with SRD error, we assume that the cross-range of the doorway is roughly at the center of the scanning path. So the estimated range is the range between the radar and the doorway midpoint, which is unbiased by averaging all the reliable range information

[4]The ranging information estimated in the open doorway detection provides only the distance between the wall and the robot, say R meters. In order to guarantee that the UGV will go through the door, the distance the UGV has to travel toward the door for more than R meters so that, when it stops, the whole robot is on the other side of the wall. In the experiments, this distance is set to be $R+1$ meters. The following is what the UGV does when it has detected the closest wall and the open doorway: a). UGV moves to the estimated mid-point of the open doorway; b) Then it turns to the direction that is perpendicular to the door; c) It moves forward by $R+1$ meters. Therefore, in this case, the 0.5 m range estimation error, which is presented in the realistic open doorway detection at low SNR region, does not affect the result a lot.

Table 4.4: Ranging Information Detection obtained from Experiment Data

True Range	SRD Error	Measured Range					
		Ideal	Trial1	Trial2	Trial3	Trial4	Trial5
69cm	0°	69cm	59.5cm	76.4cm	53.3cm	66.3cm	64.1cm
126cm	0°	126cm	148cm	132.4cm	126.2cm	120.4cm	125.6cm
310cm	0°	310cm	244.7cm	241.2cm	246.1cm	257.7cm	226.8cm
Start from 69cm	5°	87cm	99.1cm	99.3cm	99.8cm	100.4cm	98.9cm
Start from 126cm	10°	161cm	141.8cm	134.7cm	147.6cm	156.2cm	148.4cm

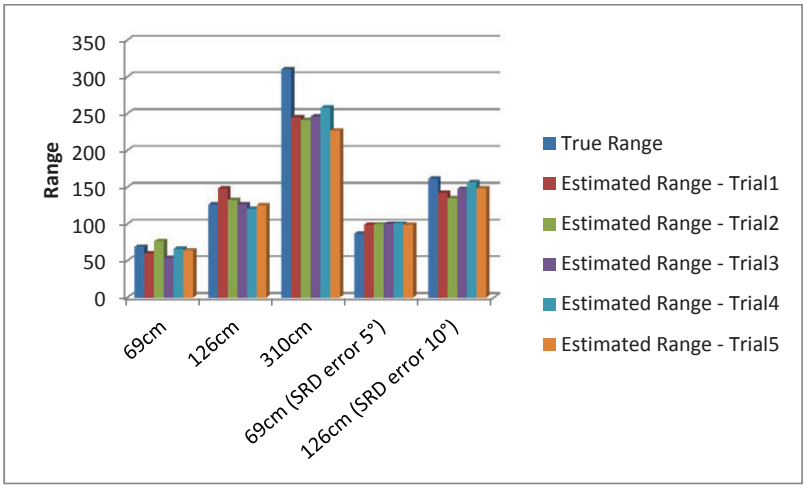

Figure 4.11: Illustration of Radar Ranging Results (Distance between the Radar and the Doorway Mid-point)

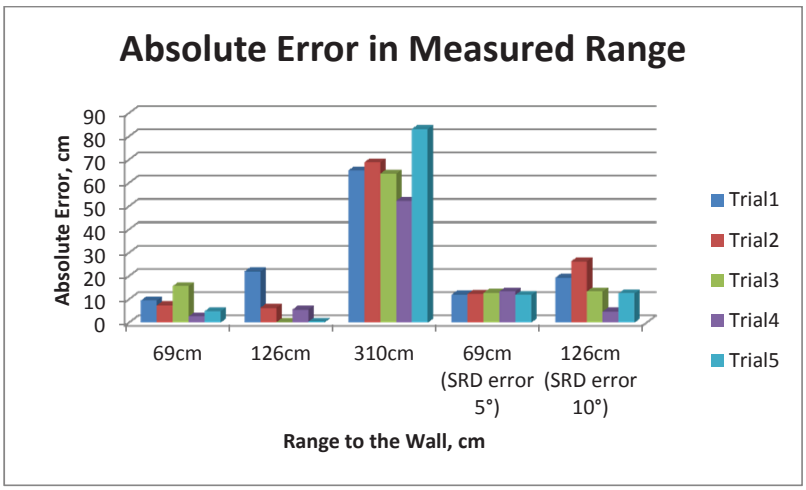

Figure 4.12: Illustration of Radar Ranging Error

4.5 Combination of Power-based Doorway Detection and Radar Ranging Information

In Section 4.3.3, the doorway position is estimated, which gives the "cross-range" information of the open doorway. In addition, the distance between the wall and

the radar (called "range" in this thesis) is investigated in Section 4.4. Therefore, if we consider the radar's starting location as the origin, the range and cross-range information of the open doorway will enable the radar to deduce the (x,y) coordinate of the doorway edges and mid-point, which is illustrated in Fig. 4.13. An example of doorway edges position coordinate in the detection case at 69 cm is shown in Fig. 4.14[5]. As can be seen, all 5 trials results in Fig.4.14 have reasonable accuracy for the range and cross-range detection of the doorway position compared with the ideal case.

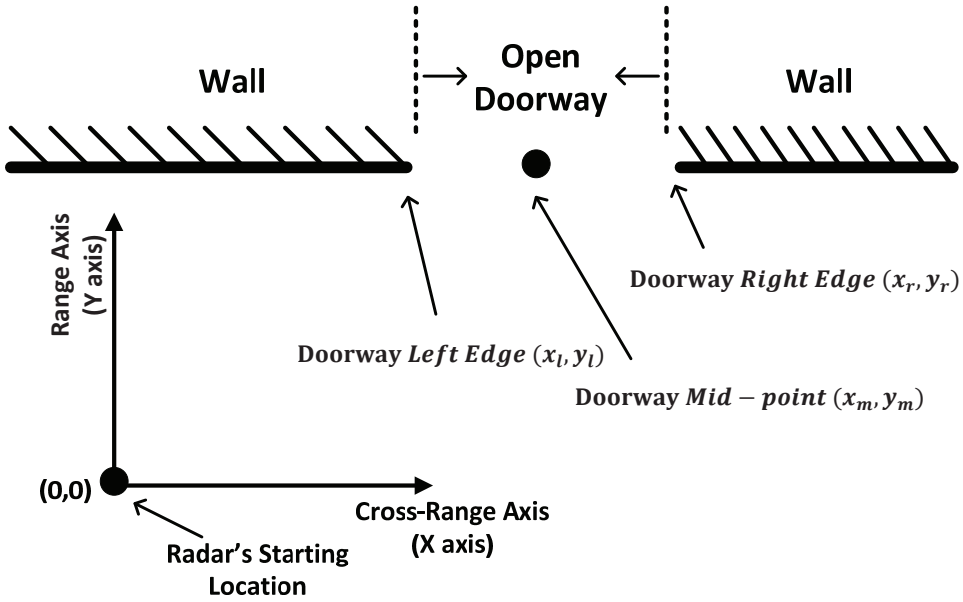

Figure 4.13: Illustration of Doorway Edges and Mid-point Coordinate Estimation

4.6 Verification of Doorway Detection Procedure

In this section, the proposed doorway detection procedure is verified in a different measurement site, which is shown in Fig. 4.15. The same parameters, i.e. $\lambda = 2.2$ and $\mu_{scale} = 0.88$, are used for the doorway position detection algorithm. The verification results are given as follows:

[5]The x-axis represents the cross-range while the y-axis denotes the range (distance between the doorway and the radar)

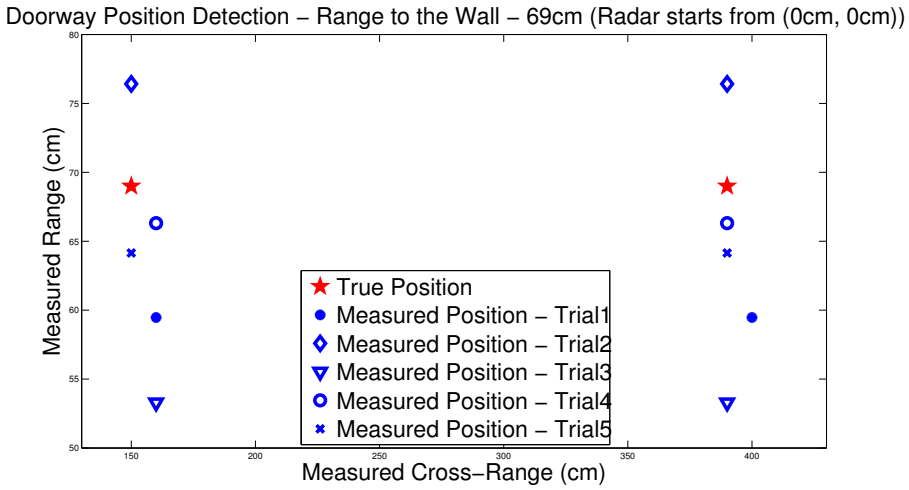

Figure 4.14: An Example of Doorway Position Coordinate

Table 4.5: Results of Verification of Doorway Detection Procedure

True Range	Measured Range	Measured Doorway Position (**True Position: 140cm-290cm**)
30cm	50.4cm	140cm-308cm
80cm	63.2cm	177cm-252cm
110cm	108.6cm	150cm-280cm
150cm	104.4cm	187cm-317cm

4.6.1 Verification of "Step 1" Measurements

In the first step, SRD is performed at the starting position in the new experiment site. An example of SRD results at 30 cm range to the wall is shown in Fig. 4.16. It shows that the SRD results follow our expectation and the error of nearest wall identification is acceptable.

4.6.2 Verification of "Step 2" Measurements

In the second step, power-based doorway detection profile is collected by scanning the nearest wall. One example of such profile at 30 cm is presented in Fig. 4.17(a) and the corresponding results obtained by using total variation de-noising are shown in Fig. 4.17(b). The de-noised profile clearly shows that the noise is smoothed out and a clear doorway is present. In Table 4.5, the doorway detection results collected at different range to the wall are presented. Further-

Figure 4.15: Experiment Site for Verification of the Doorway Detection Procedure

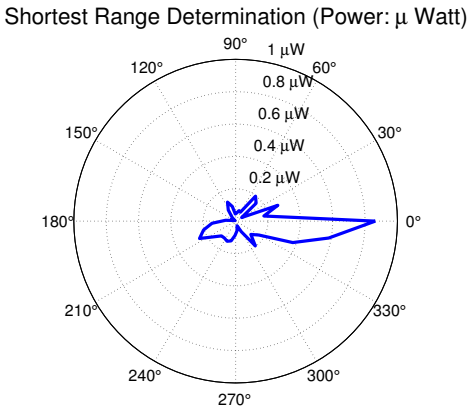

Figure 4.16: Verification of "Step 1" Measurements (Correct Nearest Wall Direction is at 0°)

more, the estimated doorway position coordinates are also plotted in Fig.4.18. It is clear that the proposed doorway detection procedure works fine in this new experiment site.

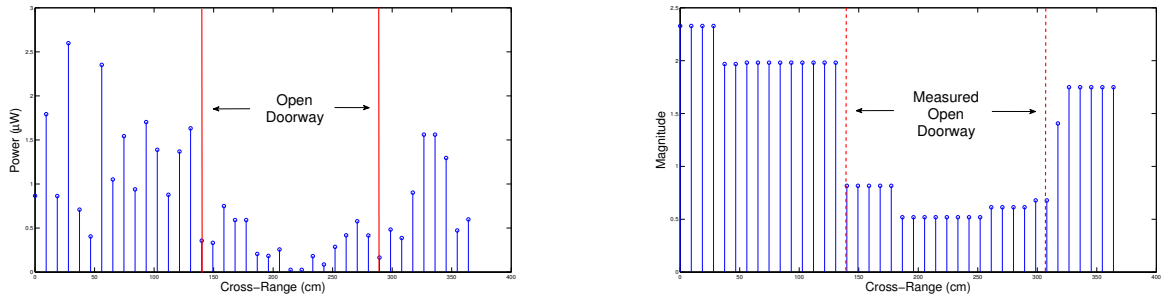

(a) Original Power-based Doorway Detection Profile (b) De-noised Power-based Doorway Detection Profile

Figure 4.17: An Example of Power-based Doorway Detection Profile at New Experiment Site

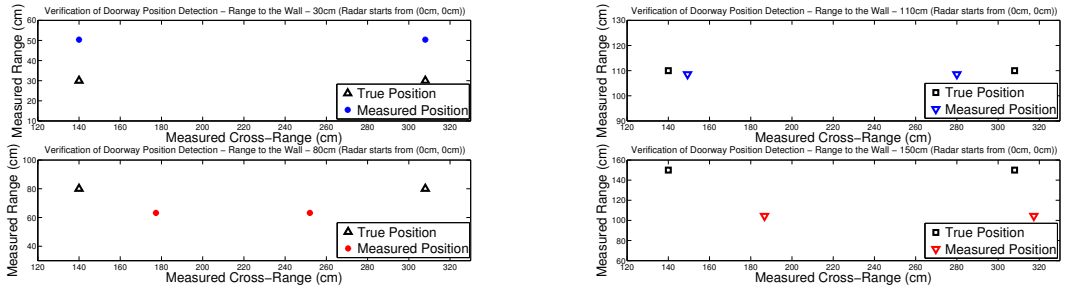

Figure 4.18: Coordinate Results of Verification of "Step 2" Measurements

4.7 Concluding Remarks

In this chapter, a "2-step" doorway detection procedure is utilized and field measurements are presented, which exhibit a detection performance with sub-meter accuracy. In "Step 1" of this procedure, the SRD is developed for the nearest wall detection. In "Step 2" of this procedure, a power-based doorway detection algorithm and a radar ranging process are combined to estimate the (x,y) coordinates of the doorway mid-point. Eventually, the proposed doorway detection procedure is verified in a different experiment site with reasonable accuracy obtained.

Moreover, the overall system performance evaluation based on the experiment results is present as follows:

- In Section 4.3.3, the doorway mid-point detection results are present. According to their errors shown in Fig. 4.10, the RMS error of doorway mid-

point detection results is 8.19 cm, which is relatively small compared with the doorway length. Therefore, the doorway mid-point detection is accurate and robust, which is also verified by the demonstration of radar-guided UGV in Section 5.3.2.

- In Section 4.4, the radar ranging process is proposed to provide extra doorway "Range" information (Range to the wall). According to the ranging errors shown in Fig. 4.12, the RMS error of radar ranging results is 32.2 cm and the large detection errors mainly come from the detection results at 310 cm range. The radar ranging error is relatively large compared with the doorway mid-point detection error. It is discussed in Section 6.2.2 that the radar ranging performance can be improved by increasing the bandwidth of radar waveform.

- In Section 4.5, the open doorway detection method and the radar ranging process were combined together to build up open doorway coordinates. The RMS error of doorway mid-point coordinates which can be evaluated based on Fig. 4.10 and Fig. 4.12 is 33.2 cm. It is very close to the RMS error of radar ranging results, which means that the main errors come from radar ranging process.

Chapter 5

Development of Radar-Guided UGV

5.1 Introduction

In this chapter, the development of a radar-guided UGV is presented, followed by the demonstration of the UGV performing the open doorway detection autonomously. In collaboration with a FYP (Final Year Project) student, we implemented a radar-guided UGV which is able to detect an open doorway in an indoor environment. As mentioned in Chapter 4, all the demonstrations were performed at the lobby on the 4th floor of Research Techno Plaza as shown in Fig. 4.1.

First, the preliminary setup of the radar-guided UGV is presented. The detailed setup of two separate systems, namely narrowband radar system and Pioneer 3-AT, are introduced along with their central controller, i.e. a computer. The setup of the entire radar-guided UGV is presented next.

Then, the demonstration of the open doorway detection is presented and discussed. The doorway detection procedure, as explained in Chapter 4, can be decomposed into 2 steps. In "Step 1", SRD is performed to detect the nearest wall. Then in "Step 2", by scanning the space parallel to the detected nearest wall, an open doorway is detected. Videos of the experiments were recorded.

5.2 System Setup of the Radar-Guided UGV

5.2.1 System Description

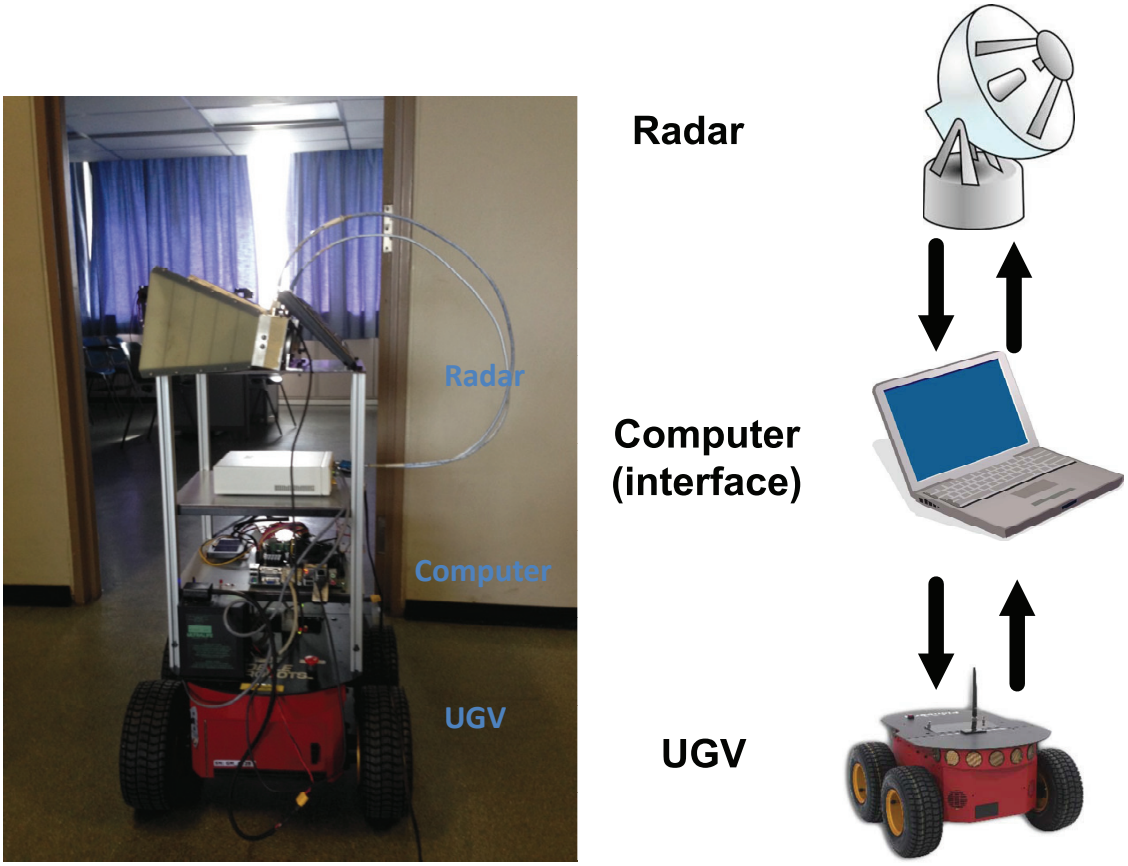

(a) Illustration of the Proposed Radar-guided UGV (b) Illustration of the Setup of Radar-guided UGV

Figure 5.1: System Setup of Radar-guided UGV

The proposed radar-guided UGV is shown in Fig. 5.1(a). It is composed of a UGV, a control unit and a radar sensor. The Pioneer 3-AT [34] is used as the UGV and the control unit is a computer. The radar sensor is constructed by using two horn antennas and one USRP[1]. The radar system performs power detection as well as radar ranging to provide the detected doorway location information, which is used by the computer to guide the UGV to go through the door. The computer plays two roles. Not only does it do all the radar signal processing works by using

[1]The attached horn antennas are facing to the left side of the UGV because we assume that the wall is on the left side of the UGV in "Step 2". Of course, it will be more flexible if the horn antennas are installed on a rotatable base.

the algorithms developed in Chapter 4, it also serves as the control unit to drive the UGV.

5.2.2 Setup of Radar System

As shown in Fig. 5.1(a), the radar system is placed on top of the UGV. Two horn antennas and a computer are connected with the USRP by using two cables and a Ethernet cable, respectively. In this way, the radar waveform samples are delivered to and received from the USRP via the Ethernet cable. The radar sensing is performed as follows:

1. The computer generates the basedband radar waveform samples and sends the samples to the USRP-based radar via Ethernet cable;

2. Digital to Analog Conversion (DAC) is performed by the USRP and then the baseband radar waveforms are modulated using a suitable carrier frequency and transmitted through the TX antenna;

3. The echo of the radar waveforms are received by the RX antenna, followed by down-conversion and Analog to Digital Conversion (ADC) operation;

4. The RX radar waveform samples are sent to the computer via Ethernet cable. Then the RX power and ranging information at current position are estimated by the method developed in Chapter 4.

5.2.3 Setup of UGV

As discussed in Section 2.4, Pioneer 3-AT platform is used as the chasis of the proposed radar-guided UGV. It is connected with the computer via a cable so that it could be controlled by using a MATLAB function (m-file), in which the movement parameters of Pioneer 3-AT such as the velocity, the angular velocity and the duration could be specified. The UGV movement is controlled as follows:

1. The velocity, the angular velocity and the movement duration are specified in a MATLAB m-file which is executed by the computer;

2. After the commands are received, Pioneer 3-AT moves according to these parameters specified in the MATLAB m-file.

5.2.4 Setup of Radar-Guided UGV

In this section, how the radar-guided UGV operates autonomously to find an open doorway is introduced. As discussed in Section 4.2, the open doorway detection can be decomposed into two steps:

- **"Step 1"** : Under the control of the computer, the UGV rotates step by step for one cycle 360° with a fixed step size, e.g. $10°/step$. In each step, the radar system performs radar sensing once (details in Section 5.2.2) and stores the RX power. Once one cycle of rotation is finished, by searching the maximum RX power, the nearest wall direction is determined. Given the direction of the nearest wall, the UGV turns to the direction at which the side of robot is parallel to that wall and then it is ready to commence to "Step 2".

- **"Step 2"** : The UGV moves forward with a fix step size, e.g. 10 cm, until the UGV gets close enough to the wall (another wall) in front. Before each step the UGV moves forward, the radar system performs the radar sensing and stores the RX power and ranging information of the current position. Once the scanning procedure is completed, the power-based doorway detection algorithm and the radar ranging processing are performed for all the collected data to estimate the doorway position. Then the UGV moves backwards to the estimated doorway mid-point and turn 90° to face the open doorway perpendicularly. Then, given the range between the radar and the door, the UGV goes through door by moving forward a distance that is larger than the estimated range.

5.3 Demonstration of the Open Doorway Detection

5.3.1 "Step 1" Demonstration

In "Step 1", SRD is used to detect the nearest wall. A video demo of "Step 1" detection of the implemented radar-guided UGV can be viewed at `https://www.youtube.com/watch?v=eGwO5oiOoLM`. The SRD error is less than 10° as shown in the video. Recalled that, in Chapter 4, the doorway detection procedure still works fine even if the SRD error is 10°. Therefore, the SRD error shown in the demo is acceptable to proceed to "Step 2" .

The rotation angle in the above video is very small (roughly 4.4°). In order to speed up the "Step 1" measurement, we could increase the rotation angle, which, however, may lead to a larger SRD error. Therefore, there is a trade off between the SRD detection time and SRD detection accuracy, which should be carefully considered in practical scenario.

5.3.2 "Step 2" Demonstration

In "Step 2", the UGV scans the space parallel to the wall by using radar. Power-based doorway detection method is used to estimate the leftmost and right most edges of the doorway, followed by a middle point calculation. Based on these information, the computer drives the UGV to go through the estimated doorway middle point[2]. The radar ranging algorithm proposed in Section 4.4 is used to estimate the distance between the UGV and the wall so that the UGV can go through the door. A video demo of the implemented radar-guided UGV can be viewed at `https://www.youtube.com/watch?v=DeBwyZWRpvw`. As shown in the video, the robot successfully detects the middle point of the doorway. Furthermore, the robot moves through the door by using the radar ranging information.

[2]The middle point is calculated by averaging the leftmost and rightmost edges of the doorway

5.3.3 Open Doorway Detection Demonstration

A complete doorway detection is demonstrated in this section. The video demo of the implemented radar-guided UGV can be viewed at `https://www.youtube.com/watch?v=CCxIJbK4FFs`. In this video recording, as there is a roughly 10° SRD error presented in "Step 1", the robot gradually moves away from the wall in "Step 2". However, the presence of an open doorway is still identified and a reasonably accurate doorway middle point is also estimated. Therefore the UGV is capable of going through the door even if a small SRD error is present.

On the other hand, in order to save the SRD detection time, sometimes a larger rotation angle is utilized, which may lead to a larger SRD error. Due to this SRD error, the direction in which the robot moves was not exactly perpendicular to the line connecting both edges of the door when it was going through the door. As a result, it may hit the edge of the door when it goes through the door if the error is significant with respect to the size of the doorway and the distance between the robot and the wall.

5.4 Concluding Remarks

In this Chapter, the setup of the radar-guided UGV is discussed in details and the proposed doorway detection procedure is demonstrated by using the Pioneer 3-AT with our proposed USRP-based radar system. Demonstrations for each step are shown, followed by a complete demonstration of the entire doorway detection procedure. The results show that the detection performance is acceptable if the SRD error in "Step 1" is below 10°.

Chapter 6

Conclusions and Future Works

6.1 Conclusions

In this thesis, we design a low cost USRP-based software defined narrowband radar system. A 2-step open-doorway detection procedure is proposed to perform indoor radar sensing by using this radar system, which could be implemented on an unmanned ground vehicle for autonomous indoor navigation in special environment such as an environment with low visibility. Field-tested experiments are carrier out and detection results are presented.

First of all, we calibrate the proposed radar system and verify the radar ranging algorithm. The TX power and RX power are carefully calibrated by using oscilloscope and signal generator respectively, followed by the direct coupling calibration in the anechoic chamber. The direct coupling effect limits the maximum detection range to around 7.1 m, which is verified in realistic indoor environment. In addition, we found out that, when the radar faces the wall (the target), the relationship between the received power and the distance to the wall follows the free-space path loss equation, rather than the traditional radar equation. This is due to the fact that the wall is too large to be treated as a point scatterer, and is better approximated by an infinite reflecting surface. Then we validate the radar ranging algorithm in three conditions, 1) with cables (to avoid multipath and self-interference problems), 2) in an anechoic chamber (to avoid multipath) and 3) in a

real indoor environment. The test results show that the mean square error of radar ranging is approximately 70 cm, which are accepted given the narrow bandwidth (10 MHz), practical sampling rate (25 MHz) of the USRP hardware as well as the usage of quadratic interpolation-based estimation algorithm.

To perform indoor open doorway detection, a "2-step" doorway detection procedure is proposed. In the first step (Step 1), the nearest wall is detected by a method called Shortest Range Determination (SRD). Then, in the second step (Step 2), by scanning parallel to the wall, an open doorway is found by a proposed doorway detection algorithm. Total variation de-noising is utilized to remove the impulse noise in this detection algorithm. By detecting the cross-range of the positions for the leftmost side and the rightmost side of the corresponding doorway, an clear open doorway is detected. The experimental results give a detection error of around 14 cm. Furthermore, we measure the distance between the wall and the radar by using radar ranging, which presents a mean square error of roughly 70 cm. The proposed doorway detection procedure is verified in 2 experiment sites.

Finally the doorway-detecting USRP-based radar is attached on a Pioneer P3-DX robot. The UGV is autonomously commanded by the USRP-based radar to find the open doorway based on the proposed 2-step detection procedure. As shown in the video recordings, the doorway position detection method works pretty well if no SRD error is presented. Moreover, the proposed radar is able to navigate the robot to go through the doorway autonomously if the SRD error presented in "Step 1" is not too severe.

In short, a preliminary design and development of a narrowband radar system for indoor doorway detection is successfully achieved and demonstrated in this MEng program. This study can be used as an initial step in the development of an inexpensive, multi-functional radar sensor for search-and-rescue missions to enhance the detection capability.

6.2 Future Works

6.2.1 Direct Coupling Cancellation

In this research, the OFDM symbols, rather than a short pulse, are utilized as the radar waveforms, so the direct coupling effect can not be removed by time gating. As found in Section 3.3, the direct coupling effect is not negligible when the detection range is above 7.1 m, which severely interferes with the echo signals. Therefore, in the future, direct coupling needs to be canceled to eliminate self-interference and enhance the detection range.

6.2.2 More Accurate Radar Ranging

In Section 3.5, we state that the sampling rate in the receiver, which is 25 MHz, gives a range accuracy of 6m. Recently, a new version of USRP named USRP X310 [40] is available. The maximum sampling rate is up to 120 MHz, which increases the ranging accuracy as discussed in Section 2.2.2. By using this USRP X310, the proposed radar system may offer more accurate radar ranging to estimate the distance between the wall and the doorway.

Moreover, in Section 5.3.1, the direction of facing nearest wall perpendicularly is detected by searching for the strongest returned power after rotating the robot for one circle. In Section 5.3.1, however, we find out that the SRD error may be severe, i.e. more than 10° due to the inaccuracy of UGV movement and fading effect. It causes the robot to move away from (or towards) the wall, instead of parallel to it. The distance between the wall and the radar has a close relationship with the SRD error and the cross-range. Therefore, if the UGV is capable of compensating the SRD error by measuring the distance to the wall at different cross-range, the robot will be able to navigate through the doorway properly even if the SRD error is non-negligible.

6.2.3 Multi-UGV Navigation and Communications

In this thesis, a single radar-based UGV is used to detect the doorway position. This UGV could share its doorway position information with nearby UGVs to perform multi-UGV navigation, which is expected to improve accuracy. Moreover, the reason why we utlize OFDM waveform as the radar waveform is that it could be fused with communications waveform. As a result, we could perform radar detection and wireless communications using the same waveform. To prevent the interference between different UGVs, different subcarriers could be assigned to different UGVs. Finally a network of UGVs could collaborate to perform navigation cooperatively in more challenging environments.

6.2.4 More Complicated Detection Environment

In this thesis, the project involved system design and algorithm development for the initial study and the study of indoor clutter was left out due to time constraints. However, in order to work properly in the realistic indoor environment, effect of radar reflection from objects, such as furniture, machines, etc, must be addressed. In the future, the radar reflection from objects need to be carefully investigated and compared with the radar reflection from the wall. We can build up a classifier to distinguish the difference between these different objects. Perhaps the integration of ranging information and the returned power information will help. Moreover, combination of different sensors should be considered as there are limited information provided by radar sensor alone. For example, ultrasonic sensors with digital (ON/OFF) outputs have excellent repeat sensing accuracy. It is possible to ignore immediate background objects e.g. the wall (object of radar), which could complement the radar sensor and detect the obstacles in front of the wall, e.g. furniture, machines. Hence fusion of different sensing modalities may greatly enhance the indoor navigation performance.

Appendix A

Horn Antenna Vs Printed Circuit Antenna

The light-weight directional printed circuit antennas, specifically, log periodic antennas (900-2600 MHz) [43], were actually considered and employed at early stages of this study. An example of the doorway detection profile using printed circuit antennas is shown in Fig. A.1. As you can see, an open doorway is detectable. However, we decided to substitute the horn antennas for the printed circuit antennas later due to the following three reasons:

First, as the beam width of the printed circuit antennas are wider than that of horn antennas, i.e. more power leakage to the sides, the direct coupling effect of printed circuit antennas is stronger. The comparison between the direct coupling power of horn antennas and printed circuit antennas of our proposed narrowband radar system is shown in Table A.1. The maximum radar sensing range (will be discussed in Section 3.4) is determined by the power of direct coupling. A stronger power of direct coupling leads to a smaller radar sensing range. Therefore, we replaced printed circuit antennas with horn antennas to improve the maximum detection range.

Second, a wider beam width of the printed circuit antennas induces more severe fading. One example of the doorway detection profile with SRD (Shortest Range Determination) error using the printed circuit antennas is shown in Fig. A.2.

Table A.1: Comparison between the Horn Antenna and the Printed Circuit Antenna

Antenna Types	TX Power	Direct Coupling Power
Printed Circuit Antenna	1.4 dBm	-34.7 dBm
Horn Antenna	1.4 dBm	-56.4 dBm

The returned signal power shows additional variations (when facing the wall) due to the severe fading effect, which presents poorer performance of open doorway detection. Hence we choose to use horn antennas to suppress the fading effect.

Third, the heavy weight of horn antennas is not a problem for the UGV that we are using now, which is Pioneer 3-AT robot [34]. So horn antennas are able to be employed to demonstrate the open doorway detection of radar-guided UGV.

In total, replacing the printed circuit antennas to the horn antennas helps us suppress the fading effect and obtain a better performance of open doorway detection without losing too much. Thus horn antennas are employed in our proposed radar system.

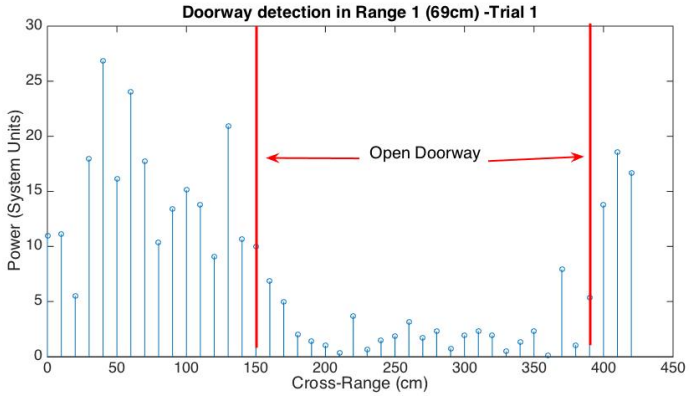

Figure A.1: Example of Doorway Detection Profile using Printed Circuit Antennas

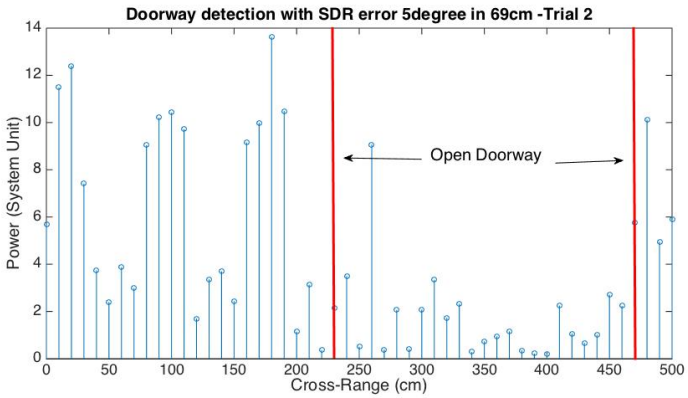

Figure A.2: Example of Doorway Detection Profile with SRD Error using Printed Circuit Antennas

Appendix B

Free Space Path Loss Model Vs Two-ray Ground Reflection Model

A two-ray ground reflection model, which considers the floor reflection, has also been considered[1]. Although the two-ray ground reflection model, which considers both the direct path and a ground reflection path as shown in Fig B.1 [41], may give a better approximation of the power model in an indoor doorway detection scenario, we found that the free space model is still good when d is small [42]. In order to quantify how small d is, a cross-over distance d_c is defined as:

$$d_c = \frac{(4\pi h_t h_r)}{\lambda} \tag{B.1}$$

where h_t and h_r are the heights of the transmit and receive antennas, respectively while λ is the wavelength.

When $d < d_c$, free space path loss model is used. On the other hand, when $d > d_c$, two-ray ground reflection is used. According to (B.1), the cross-over distance of our experiment setup[2] is 30 m. As discussed in Section 3.4, the detection range for our indoor doorway detection scenario is less than 7.1 m. Consequently

[1]Note that the original free space propagation scenario shown in Fig. B.1 can be easily generalized into the indoor doorway detection scenario by inserting a reflection factor to the formula as we will discuss in Section 3.4.

[2]The heights of both transmitter and receiver are roughly 0.6 m while the wavelength is 0.15 m

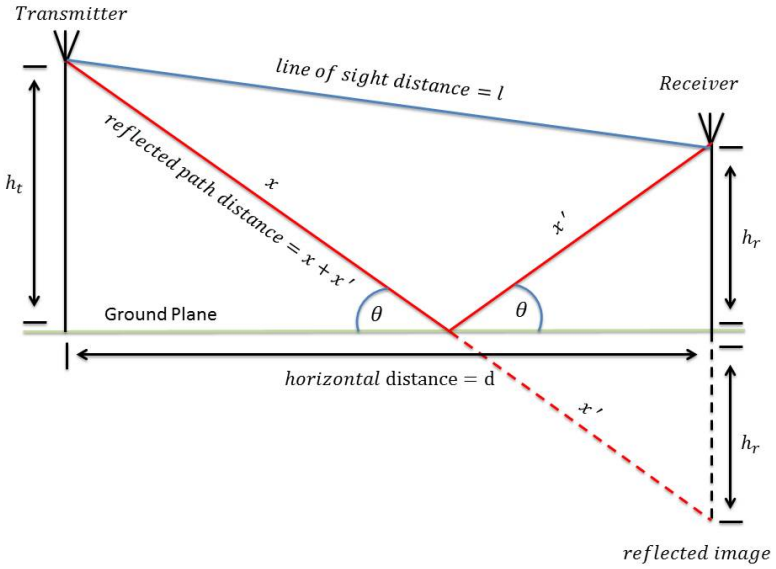

Figure B.1: Two Ray Ground Reflection Model

the power model of our indoor doorway detection scenario is better approximated by free space path loss model, rather than two-ray ground reflection model.

Bibliography

[1] N. A. Rawashdeh and H. T. Jasim, "Mult-sensor input path planning for an autonomous ground vehicle," in *Mechatronics and its Applications (ISMA), 2013 9th International Symposium on IEEE*, pp. 1–6.

[2] R. Labayrade, D. Aubert, and J.-P. Tarel, "Real time obstacle detection in stereovision on non flat road geometry through" v-disparity" representation," in *Intelligent Vehicle Symposium, 2002. IEEE*, vol. 2, pp. 646–651.

[3] I. Ulrich and I. Nourbakhsh, "Appearance-based obstacle detection with monocular color vision," in *AAAI Nat. Conf. on Artificial Intelligence*, 2000, pp. 866–871.

[4] G. Y. Jiang, T. Y. Choi, S. K. Hong, J. W. Bae, and B. S. Song, "Lane and obstacle detection based on fast inverse perspective mapping algorithm," in *IEEE Int. Conf. Systems, Man, Cybernetics, vol. 4, 2000*, vol. 4, pp. 2969–2974.

[5] D. Amarasinghe, G. K. Mann, and R. G. Gosine, "Moving object detection in indoor environments using laser range data," in *Proceedings of the 2006 IEEE International Conference on C Intelligent Robots and Systems, Oct. 2006*, pp. 802–807.

[6] Z. Xu, Y. Zhuang, and H. Chen, "Obstacle detection and road following using laser scanner," in *Proceedings of the 6th World Congress on Intelligent Control and Automation, Dalian, China*, vol. 2, pp. 8630–8634.

[7] B. Jameson, D. Garmatyuk, and Y. J. Morton, "Cognitive radar for indoor positioning with a software-defined UWB OFDM system," in *Radar Conference (RADAR), 2012 IEEE*, pp. 0465–0470.

[8] B. Jameson, D. Garmatyuk, Y. Morton, K. Kauffman, and R. Ewing, "Reconnaissance using adaptive multi-carrier radar," in *Radar Conference (RADAR), 2013 IEEE*, pp. 1–6.

[9] R. Cole, B. Jameson, D. Garmatyuk, and Y. Morton, "Simultaneous indoor localization and detection with multi-carrier radar," in *Radar Conference (RADAR), 2014 IEEE*, pp. 0881–0886.

[10] Z. Tong, M. Arifianto, and C. Liau, "Wireless transmission using universal software radio peripheral," in *Internationsl conference on Space Science and Communication, Malaysia*, pp. 19–23.

[11] A. Mate, K.-H. Lee, and I.-T. Lu, "Spectrum sensing based on time covariance matrix using GNU radio and USRP for cognitive radio," in *Systems, Applications and Technology Conference (LISAT), 2011 IEEE Long Island, 2011*, pp. 1–6.

[12] J. Blumenstein and Z. Fedra, "The 2D spreading based communication systems implementation using USRP," in *Radioelektronika (RADIOELEKTRONIKA), 2010 20th International Conference*, pp. 1–4.

[13] A. Martian, L. Petrica, and O. Radu, "Cognitive radio testing framework based on USRP," in *Telecommunications Forum (TELFOR), 2013 21st*, pp. 212–215.

[14] X. Shi and R. de Francisco, "Adaptive spectrum sensing for cognitive radios: an experimental approach," in *Wireless Communications and Networking Conference (WCNC), 2011 IEEE*, pp. 1408–1413.

[15] F. Berizzi, M. Martorella, D. Petri, M. Conti, and A. Capria, "USRP technology for multiband passive radar," in *Radar Conference (RADAR), 2010 IEEE*, pp. 225–229.

[16] A. Prabaswara, A. Munir, and A. B. Suksmono, "GNU Radio based software-defined FMCW radar for weather surveillance application," in *Telecommunication Systems, Services, and Applications (TSSA), 2011 6th International Conference on IEEE*, pp. 227–230.

[17] M. Braun, M. Müller, M. Fuhr, and F. K. Jondral, "A USRP-based Testbed for OFDM-based Radar and Communication Systems," in *Proc. of 22nd VTech Symposium on Wireless Communications, 2012*.

[18] "Radar Wikipedia," http://en.wikipedia.org/wiki/Radar.

[19] "Radar Range Resolution," http://www.radartutorial.eu/01.basics/Range%20Resolution.en.html.

[20] A. Goldsmith, *Wireless communications*. Cambridge university press, 2005.

[21] S. M. Kay, *Fundamentals of Statistical Signal Processing: Estimation Theory*. Upper Saddle River, NJ, USA: Prentice-Hall, Inc., 1993.

[22] G. Sinan, T. Zhi, B. Giannakis Georgios *et al.*, "Localization via ultra-wideband radios," *IEEE, Signal Processing Magazine*, vol. 35, no. 2, pp. 131–135, 2005.

[23] C. Cook, *Radar signals: an introduction to theory and application*. Elsevier, 2012.

[24] H. V. Poor, *An introduction to signal detection and estimation*. Springer Science & Business Media, 1994.

[25] N. El Gemayel, S. Koslowski, F. K. Jondral, and J. Tschan, "A low cost tdoa localization system: Setup, challenges and results," in *Positioning Navigation and Communication (WPNC), 2013 10th Workshop on*. IEEE, 2013, pp. 1–4.

[26] "Free Space Path Loss," http://en.wikipedia.org/wiki/Free-space_path_loss.

[27] "Radar Basics," http://www.radartutorial.eu/index.en.html.

[28] "USRP N210 Datasheet," https://www.ettus.com/content/files/07495_Ettus_N200-210_DS_Flyer_HR_1.pdf.

[29] "WBX Daughter Manual," http://files.ettus.com/manual/page_dboards.html#dboards_wbx.

[30] "USRP Wikipedia," http://en.wikipedia.org/wiki/Universal_Software_Radio_Peripheral.

[31] "USRP N210," https://www.ettus.com/product/details/{UN210-KIT}.

[32] "Horn Antenna," http://www.e-powerdevices.com/pdf/e-pwrBroadbandWGHornAntennaCatalog.pdf.

[33] "Code Example Provided with UHD," http://www.ettusresearch.com/content/files/kb/application_note_uhd_examples.pdf.

[34] "Pioneer 3-AT," http://www.mobilerobots.com/ResearchRobots/P3AT.aspx.

[35] "Robot Operating System," http://www.ros.org/about-ros/.

[36] "Robot Operating System (ROS) Support from MATLAB ," http://www.mathworks.com/hardware-support/robot-operating-system.html.

[37] "Wiki of Total Variation De-noising," http://en.wikipedia.org/wiki/Total_variation_denoising.

[38] M. A. Little and N. S. Jones, "Sparse bayesian step-filtering for high-throughput analysis of molecular machine dynamics," in *Acoustics Speech and Signal Processing (ICASSP), 2010 IEEE International Conference on*. IEEE, 2010, pp. 4162–4165.

[39] "Software Defined Radio Hardware Survey," http://people.bu.edu/mrahaim/NEWSDR/Presentations/NEWSDR_Johnston.pdf.

[40] "USRP X310," http://www.ettus.com/product/details/X310-KIT.

[41] "Wiki - Two-ray Ground Reflection Model," http://en.wikipedia.org/wiki/Two-ray_ground-reflection_model.

[42] K. Fall and K. Varadhan, "The ns manual (formerly ns notes and documentation)," *The VINT project*, vol. 47, 2005.

[43] "Printed Circuit Board Antenna - Log Periodic 900-2600 MHz," http://www.wa5vjb.com/products1.html.